

RESEARCH ARTICLE

Chronic hepatitis B virus and liver fibrosis: A mathematical model

Avner Friedman¹, Nourridine Siewe^{2*}

1 Mathematical Biosciences Institute & Department of Mathematics, The Ohio State University, Columbus, Ohio, United States of America, **2** National Institute for Mathematical and Biological Synthesis, University of Tennessee, Knoxville, Tennessee, United States of America

* nourridine@aims.ac.za



Abstract

Hepatitis B virus (HBV) infection is a liver disorder that can result in cirrhosis, liver failure and hepatocellular carcinoma. HBV infection remains a major global health problem, as it affects more 350 million people chronically and kills roughly 600,000 people annually. Drugs currently used against HBV include IFN- α that decreases viremia, inflammation and the growth of liver fibrosis, and adefovir that decreases the viral load. Each of these drugs can have severe side-effects. In the present paper, we consider the treatment of chronic HBV by a combination of IFN- α and adefovir, and raise the following question: What should be the optimal ratio between IFN- α and adefovir in order to achieve the best ‘efficacy’ under constraints on the total amount of the drugs; here the efficacy is measured by the reduction of the levels of inflammation and of fibrosis? We develop a mathematical model of HBV pathogenesis by a system of partial differential equations (PDEs) and use the model to simulate a ‘synergy map’ which addresses the above question.

OPEN ACCESS

Citation: Friedman A, Siewe N (2018) Chronic hepatitis B virus and liver fibrosis: A mathematical model. PLoS ONE 13(4): e0195037. <https://doi.org/10.1371/journal.pone.0195037>

Editor: Giovanni Sitia, Ospedale San Raffaele, ITALY

Received: September 21, 2017

Accepted: March 15, 2018

Published: April 10, 2018

Copyright: © 2018 Friedman, Siewe. This is an open access article distributed under the terms of the [Creative Commons Attribution License](https://creativecommons.org/licenses/by/4.0/), which permits unrestricted use, distribution, and reproduction in any medium, provided the original author and source are credited.

Data Availability Statement: All relevant data are within the paper and its Supporting Information files.

Funding: This research was supported by the Mathematical Biosciences Institute of The Ohio State University. This work was conducted while Nourridine Siewe was a Postdoctoral Fellow at the National Institute for Mathematical and Biological Synthesis, an Institute sponsored by the National Science Foundation through NSF Award #DBI-1300426, with additional support from The University of Tennessee, Knoxville.

Introduction

Hepatitis B virus (HBV) infection is a liver disorder that can result in cirrhosis, liver failure, and hepatocellular carcinoma; it is one of the most prevalent infectious diseases associated with human liver diseases, including acute, fulminant and chronic hepatitis [1]. Despite the availability of HBV vaccine and the development of antiviral therapies, HBV infection remains a major global health problem. Chronic HBV affects more than 350 million people of whom roughly 600,000 die annually from HBV-related liver diseases [1–3].

To understand the virus biology and pathogenesis in HBV-infected patients, several animal models have been developed to mimic hepatic HBV infection and the immune response against HBV [1, 4, 5]. However, as observed in [1], the narrow host range of HBV infection and lack of a full immune response spectrum in animal models remain significant limitations. For this reason, it may be useful to develop a mathematical model of the progression of HBV, which includes the host response to treatment. In the present paper we introduce such a model and use it to study the effect of a combination therapy with two currently used drugs, interferon alpha (IFN- α) [5–7] and adefovir [8–11]. The model shows that it may be possible

Competing interests: The authors have declared that no competing interests exist.

to reduce HBV infection and viral load while, at the same time, decrease inflammation and control liver fibrosis.

Monotherapy of HBV infection with IFN- α decreases viremia, inflammation and the progression of liver fibrosis. However, only a small fraction of patients respond positively to treatment [5, 6]. Monotherapy with adefovir decreases the viral load by blocking reverse transcriptase, an enzyme that is crucial for the reproduction of HBV in the body [8, 12, 13].

Both IFN- α and adefovir can have severe side-effects when administered alone, including brain disorder that may lead to a stroke, a heart attack or lung fibrosis for IFN- α [14], and kidney damage, a low amount of phosphate in the blood, a stroke or pancreatitis for adefovir [15]. A combination therapy with smaller dose may be as effective, or even more effective, than monotherapy with a larger dose if there is a 'positive synergy' between the two drugs. We shall use our mathematical model to determine the synergy between IFN- α and adefovir.

In their study of HBV infection in a humanized mouse model where the mice are inoculated with clinical isolates HBV *in vivo*, the authors in [16] showed that a persistence of liver disease due to HBV infection is associated with infiltration of M2 macrophages. They found that chronic HBV infection in the liver of humanized mice is associated with human hepatic stellate cells (HSCs) activation/infection and human liver fibrosis. It was also observed in [16] that infection of M1 and M2 macrophages with HBV results in increasing level of IL-10 and decreasing level of IL-12. Although the authors in [16] do not demonstrate that HBV infects macrophages, they show that inoculation of macrophage cultures with HBV results in macrophage activation, however the mechanism of activation is unknown. Since the possibility that HBV could infect macrophages remains to be conclusively proven, we do not assume that macrophage infection is a major source of virus as compared to HSCs.

Methods

In the course of chronic HBV infection, M1 macrophages produce pro-inflammatory cytokines IL-6 [17–19], IL-12 [17, 20, 21] and TNF- α [22, 23], while M2 macrophages produce anti-inflammatory cytokines IL-1 β [17, 18, 20, 24], IL-4 [25, 26], IL-10 [17–19, 27, 28], IL-13 [17–19, 27–29] and TGF- β [30], and chemokine PDGF [31, 32]. The HBV environment includes T cells: Th1 and Th2. Th1 is activated by IL-12 [33] and it produces IL-2 [17], IFN- α [34] and IFN- γ [17, 20, 35]. Th2 is activated by IL-4 [36]. Th2 is activated by IL-4 [37] and it produces IFN- α [38], IL-4 [25, 26], IL-10 [27, 28] and IL-13 [27, 28, 39]. Th1 and Th2 are mutually antagonistic [36, 40, 41]. In addition to macrophages and T cells, the mathematical model will include other types of cells closely associated with chronic HBV: hepatic stellate cells (HSCs), fibroblasts and myofibroblasts. HSCs enhance the proliferation of fibroblasts by producing hyaluronic acid [42–44]. Fibroblasts are transformed into myofibroblasts by PGDF and TGF- β [30, 45–47]. Fibroblast and, more effectively, myofibroblast, produce collagen [47–50]. MMP produced by M2 macrophages disrupts collagen cross-linking and increases scarring, especially under excessive collagen concentrations [31, 32, 51]. Since M2 macrophages produce TGF- β and PDGF which enhance the presence of fibroblasts, M2 macrophages contribute to the progression of fibrosis. In chronic HBV, the virus infects both M1 and M2 macrophages, as well as hepatic stellate cells. The infected cells secrete C-C Motif Chemokine Ligand 3 (CCL3) [45, 52, 53] which attracts macrophages into the liver [31, 54], resulting in increased inflammation. The replication of the intracellular virus is blocked by several cytokines, including IFN- α , TNF- α , TGF- β and IFN- γ [20, 35, 55].

A schematic diagram of our model is shown in Fig 1, where the nodes are defined in Table 1. We represent the cells by square nodes, but the fibrosis formation pathway by diamond nodes, and the virus and cytokines by circular nodes. The nodes with reddish colors

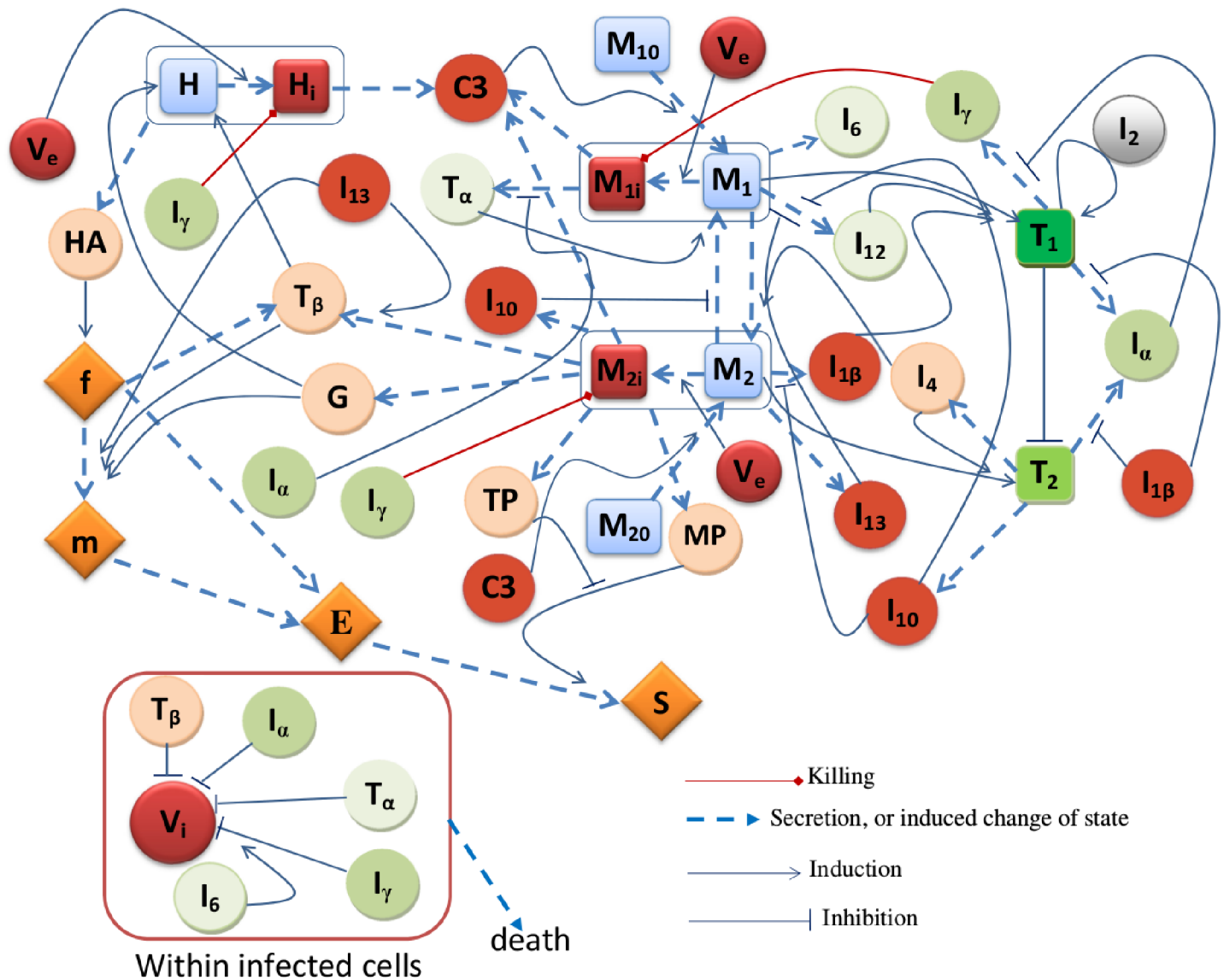


Fig 1. Diagram of interactions between cells, virus and cytokines in hepatitis B.

<https://doi.org/10.1371/journal.pone.0195037.g001>

(red and orange) indicate the variables that include and/or induce infection or fibrosis formation. the nodes with greenish colors (blue, green and silver) indicate the variables that counteract the infection. We shall use our model to compare the efficacy of treatment by a single agent (IFN- α or adefovir) with a combination, whereby the amount of each agent is less than in the monotherapy. We shall accordingly develop a ‘synergy map’ which addresses the question of achieving a desired target of efficacy in a combination therapy while using the smallest dose of these two drugs.

Mathematical models for population dynamics of HBV transmission have been developed [56–63]. In [62], the authors used a SEIR-type mathematical model by a system of ordinary differential equations (ODEs) to study the dynamics of HBV infection under administration of vaccination and treatment. A compartmental mathematical model by a system of partial

Table 1. Variables of the model. All densities and concentrations are in units of g/cm³.

Variables	Descriptions	Variables	Descriptions
H	density of healthy HSCs	H_i	density of infected HSCs
M_1	density of healthy M1 macrophages	M_{1i}	density of infected M1 macrophages
M_2	density of healthy M2 macrophages	M_{2i}	density of infected M2 macrophages
T_1	Th1 cell density	T_2	Th2 cell density
f	density of fibroblast	m	density of myofibroblast
ρ	density of ECM	S	scar density
V_e	density of external virus	V_{i2}	density of virus in M_{2i}
V_{i1}	density of virus in M_{1i}	V_{iH}	density of virus in H_i
G	concentration of PDGF	H_A	concentration of hyaluronic acid
$I_{1\beta}$	concentration of IL-1 β	I_2	concentration of IL-2
I_4	concentration of IL-4	I_6	concentration of IL-6
I_{10}	concentration of IL-10	I_{12}	concentration of IL-12
I_{13}	concentration of IL-13	I_α	concentration of IFN- α/β
I_γ	concentration of IFN- γ	T_α	concentration of TNF- α
T_β	concentration of TGF- β	M_P	concentration of MMP
T_P	concentration of TIMP	C_3	concentration of CCL3

<https://doi.org/10.1371/journal.pone.0195037.t001>

differential equations (PDEs) to predict the dynamics of HBV transmission and evaluate the long-term effectiveness of the vaccination program was developed in [63]. Another class of models that consider uninfected hepatocytes, infected hepatocytes and free virus have been developed to analyze changes in HBV levels during drug therapy [56–61]. Techniques in [58, 59] were used in [56, 60, 61] to develop mathematical models by a system of ordinary differential equations to understand the factors that govern HBV infection dynamics, and to analyze the immune mechanisms responsible for viral clearance in the case of acute HBV infection. They found that the viral load initially increases exponentially, then decreases and seems to approach a plateau after some time. Interestingly, they obtained that the number of infected cells, the number of uninfected cells and the number of CD8⁺ T cells increase in acute HBV infection, leading to clearance of the viral load. A more recent model by Friedman and Hao [64] uses reaction-diffusion equations to study the evolution of fibrosis in the liver, without specifically targeting the cause of the disease.

Mathematical model

In this section, we develop a mathematical model of liver fibrosis due to infection by HBV. In our model that builds on the model in [64], infection takes place in some region Ω of the liver. The variables used in the model are given in Table 1. These variables satisfy a system of PDEs in Ω .

Equation for macrophage density. The equation for the density of healthy M1 macrophages, not yet including a source, is given by

$$\frac{\partial M_1}{\partial t} - D_M \Delta M_1 = \underbrace{-\nabla \cdot (M_1 \chi_{C_3} \nabla C_3)}_{\text{chemotaxis}} + \underbrace{\lambda_{M_2 M_1} \frac{\epsilon_1}{\epsilon_1 + \epsilon_2} M_2}_{M_2 \rightarrow M_1} - \underbrace{\lambda_{M_1 M_2} \frac{\epsilon_2}{\epsilon_1 + \epsilon_2} M_1}_{M_1 \rightarrow M_2} - \underbrace{\lambda_{M_1 M_{1i}} V_e M_1}_{M_1 \rightarrow M_{1i}} - \underbrace{\mu_{M_1} M_1}_{\text{death}}$$

where

$$\begin{aligned} \epsilon_1 &= \left(\lambda_{MI_\gamma} \frac{I_\gamma}{I_\gamma + K_\gamma} + \lambda_{MT_z} \frac{T_z}{T_z + K_{T_z}} \right) \frac{1}{1 + I_{10}/\tilde{K}_{10}}, \\ \epsilon_2 &= \lambda_{MI_4} \frac{I_4}{I_4 + K_4} + \lambda_{MI_{13}} \frac{I_{13}}{K_{13} + I_{13}}. \end{aligned}$$

The term $\nabla \cdot (M_1 \chi_{C_3} \nabla C_3)$ is the chemotactic effect of C_3 on M1 macrophages; χ_{C_3} is the chemotactic coefficient. M2 macrophages can become M1 macrophages under the influence of IFN- γ and TNF- α , a process resisted by IL-10 [65–67], and M1 macrophages can become M_2 macrophages under the influence of IL-4 and IL-13 [29, 68]. The fourth term on the right-hand side is the infection of M1 macrophages by external virus, V_e .

Infected cells produced chemokine CCL3 [45, 52, 53] in order to attract immune response. Monocytes circulate in the blood. They are attracted to the liver tissue by CCL3 [31, 54], and then they differentiate into either M1 or M2 macrophages [69–71]. We denote M_{10} and M_{20} the densities of the monocytes from the vascular system which differentiate into M1 and M2 macrophages, respectively. Accordingly, on the boundary of each blood capillary, there is an influx of M1 macrophages into the tissue,

$$D_M \frac{\partial M_1}{\partial n} + \tilde{\beta}(C_3)(M_{10} - M_1) = 0,$$

where $\tilde{\beta}(C_3)$ is an increasing function of C_3 . Using a homogenization method as in [52], we can replace the boundary conditions on the blood capillaries by a source term in the tissue, which we take to be $\beta(C_3) = \beta \frac{C_3}{K_{C_3} + C_3}$, where K_{C_3} is a constant. Hence the final equation for the density of M1 macrophages is the following:

$$\begin{aligned} \frac{\partial M_1}{\partial t} - D_M \Delta M_1 &= \underbrace{\beta(C_3)(M_{10} - M_1)}_{\text{chemotaxis}} - \underbrace{\nabla \cdot (M_1 \chi_{C_3} \nabla C_3)}_{\text{chemotaxis}} + \underbrace{\lambda_{M_2 M_1} \frac{\epsilon_1}{\epsilon_1 + \epsilon_2} M_2}_{M_2 \rightarrow M_1} \\ &\quad - \underbrace{\lambda_{M_1 M_2} \frac{\epsilon_2}{\epsilon_1 + \epsilon_2} M_1}_{M_1 \rightarrow M_2} - \underbrace{\lambda_{M_1 M_{1i}} V_e M_1}_{M_1 \rightarrow M_{1i}} - \underbrace{\mu_{M_1} M_1}_{\text{death}}. \end{aligned} \tag{1}$$

The density M_{1i} of infected M1 macrophage satisfies the following equation:

$$\frac{\partial M_{1i}}{\partial t} - D_M \Delta M_{1i} = \underbrace{\lambda_{M_1 M_{1i}} V_e M_1}_{M_1 \rightarrow M_{1i}} - \underbrace{\mu_{M_1} (1 + \mu_{V_{il}} V_{il}) M_{1i}}_{\text{death}}, \tag{2}$$

where we assume that the death rate of M_{1i} is increased due to the viral load represented by $\mu_{V_{il}} V_{il}$.

The density of healthy M2 macrophages satisfies an equation similar to Eq (1):

$$\begin{aligned} \frac{\partial M_2}{\partial t} - D_M \Delta M_2 &= \underbrace{\beta(C_3)(M_{20} - M_2)}_{\text{source}} - \underbrace{\nabla \cdot (M_2 \chi_{C_3} \nabla C_3)}_{\text{chemotaxis}} + \underbrace{\lambda_{M_1 M_2} \frac{\epsilon_2}{\epsilon_1 + \epsilon_2} M_1}_{M_1 \rightarrow M_2} \\ &\quad - \underbrace{\lambda_{M_2 M_1} \frac{\epsilon_1}{\epsilon_1 + \epsilon_2} M_2}_{M_2 \rightarrow M_1} - \underbrace{\lambda_{M_2 M_{2i}} V_e M_2}_{M_2 \rightarrow M_{2i}} - \underbrace{\mu_{M_2} M_2}_{\text{death}} \end{aligned} \tag{3}$$

The third, fourth and fifth terms in the right-hand side of Eq (3) are complementary to the corresponding terms in Eq (1).

The density M_{2i} of infected M2 macrophages satisfies an equation similar to Eq (2):

$$\frac{\partial M_{2i}}{\partial t} - D_M \Delta M_{2i} = \underbrace{\lambda_{M_2 M_{2i}} V_e M_2}_{M_2 \rightarrow M_{2i}} - \underbrace{\mu_{M_2} (1 + \mu_{V_{i2}} V_{i2}) M_{2i}}_{\text{death}}, \tag{4}$$

where we assume that the death rate of M_{2i} is increased due to the viral load $\mu_{V_{i2}} V_{i2}$.

Equations for hepatic stellate cells (HSCs) density. In homeostasis, HSCs have a source A_H and death rate μ_H . In HBV, the proliferation of the healthy population of HSCs is enhanced by PDGF and TGF- β [45, 53, 72] and is reduced when they become infected by the extracellular virus. Hence the equation for H is the following:

$$\frac{\partial H}{\partial t} - D_H \Delta H = \underbrace{A_H}_{\text{source}} + \underbrace{\left(\lambda_{HG} \frac{G}{G + K_G} + \lambda_{HT\beta} \frac{T_\beta}{T_\beta + K_{T\beta}} \right) H}_{\text{proliferation}} - \underbrace{\lambda_{HH_i} V_e H}_{H \rightarrow H_i} - \underbrace{\mu_H H}_{\text{death}} \tag{5}$$

The infected HSCs satisfy the equation

$$\frac{\partial H_i}{\partial t} - D_H \Delta H_i = \underbrace{\lambda_{HH_i} V_e H}_{H \rightarrow H_i} - \underbrace{\mu_H (1 + \mu_{V_{iH}} V_{iH}) H_i}_{\text{death}}, \tag{6}$$

where the death rate of infected HSCs is increased due to the viral load $\mu_{V_{iH}} V_{iH}$.

Equations for T cells density. Th1 cells are activated from naive T cells (T_0) by contact with M1 macrophages, under IL-12 environment [33]; this process is resisted by IL-10 and IL-13 [17, 73]. IL-2 enhances the proliferation of Th1 cells [17, 65]. Hence the equations for the densities of Th1 and Th2 cells are given as follows:

$$\frac{\partial T_1}{\partial t} - D_T \Delta T_1 = \underbrace{\left(\lambda_{T_1 M_1} T_0 \frac{M_1}{M_1 + K_{M_1}} \frac{I_{12}}{I_{12} + K_{I_{12}}} \frac{1}{1 + I_{10}/\tilde{K}_{10}} + \lambda_{T_1 I_2} \frac{I_2}{I_2 + K_2} T_1 \right) \frac{1}{1 + I_{13}/\tilde{K}_{13}}}_{\text{activation}} - \underbrace{\mu_{T_1} T_1}_{\text{death}} \tag{7}$$

T_0 cells in the liver may also be activated into Th2 cells (T_2) by contact with M_2 in an I_4 environment [36]. The activation of T_2 is antagonized by T_1 [36, 40, 41].

$$\frac{\partial T_2}{\partial t} - D_T \Delta T_2 = \underbrace{\lambda_{T_2 M_2} T_0 \frac{M_2}{M_2 + K_{M_2}} \frac{I_4}{I_4 + K_4} \frac{1}{1 + T_1/\tilde{K}_{T_1}}}_{\text{activation}} - \underbrace{\mu_{T_2} T_2}_{\text{death}} \tag{8}$$

Equations for fibroblast (f) and myofibroblast (m) densities. Hyaluronic acid (H_A) enhances the proliferation of fibroblasts [44]. Fibroblasts are transformed into myofibroblasts

by G and T_β [30, 46, 47, 74, 75]. Hence equations of f and m are:

$$\frac{\partial f}{\partial t} - D_f \Delta f = \underbrace{\lambda_{fH_A} \frac{H_A}{H_A + K_{H_A}} f}_{\text{activation}} - \underbrace{\left(\lambda_{mfT_\beta} \frac{T_\beta}{T_\beta + K_{T_\beta}} + \lambda_{mfG} \frac{G}{G + K_G} \right) f}_{f \rightarrow m} - \underbrace{\mu_f f}_{\text{death}} \quad (9)$$

$$\frac{\partial m}{\partial t} - D_m \Delta m = \underbrace{\left(\lambda_{mfT_\beta} \frac{T_\beta}{T_\beta + K_{T_\beta}} + \lambda_{mfG} \frac{G}{G + K_G} \right) f}_{f \rightarrow m} - \underbrace{\mu_m m}_{\text{death}} \quad (10)$$

Equations for ECM (ρ) and scar (S) densities. The ECM consists primarily of fibrillar collagens and elastins, but it includes also fibronectins, lamina and nitrogen that support the matrix network by connecting or linking collagens [49]. For simplicity we represent the ECM by the density of collagens. ECM is produced by f , m and by HSCs [47, 48]. The production of ECM by m is enhanced by T_β [47, 50]. We assume that MMP degrades the ECM at a rate proportional to $M_p \rho$. Hence the equation of ρ is as follows:

$$\frac{d\rho}{dt} = \underbrace{\lambda_{\rho f} f \left(1 - \frac{\rho}{\rho_0} \right)^+ + \lambda_{\rho m} \left(1 + \lambda_{\rho T_\beta} \frac{T_\beta}{T_\beta + K_{T_\beta}} \right) m + (\lambda_{\rho H} H + \lambda_{\rho H_i} H_i)}_{\text{production}} - \underbrace{d_{\rho M_p} M_p \rho}_{\rho \rightarrow S} - \underbrace{\mu_\rho \rho}_{\text{death}} \quad (11)$$

where $\left(1 - \frac{\rho}{\rho_0} \right)^+ = 1 - \frac{\rho}{\rho_0}$ if $\rho < \rho_0$, $\left(1 - \frac{\rho}{\rho_0} \right)^+ = 0$ if $\rho \geq \rho_0$.

Fibrotic diseases are characterized by excessive scarring due to excessive production and deposition of ECM and disruption of normal healthy protein cross-linking. MMP disrupt collagen cross-linking and increases scarring in cases of excessive collagen concentrations [51]. Accordingly we model the growth of a scar as, in [51], by the formula

$$S = \lambda_S (\rho - \rho^*)^+ \left(1 + \lambda_{SM_p} \frac{M_p}{M_p + K_{M_p}} \right), \quad (12)$$

where ρ^* is the concentration of collagen in normal healthy tissue.

Equations for cytokines and other proteins.

PDGF (G) is produced by M_2 [31, 32]. Hence,

$$\frac{\partial G}{\partial t} - D_G \Delta G = \underbrace{\lambda_{GM_2} M_2 + \lambda_{GM_{2i}} M_{2i}}_{\text{production}} - \underbrace{\mu_G G}_{\text{degradation}} \quad (13)$$

Hyaluronic acid (H_A) is produced by HSCs and is degraded by sinusoidal epithelial cells [42, 43]. Hence H_A satisfies the following equation

$$\frac{\partial H_A}{\partial t} - D_{H_A} \Delta H_A = \underbrace{\lambda_{H_A H} H + \lambda_{H_A H_i} H_i}_{\text{production}} - \underbrace{\mu_{H_A} H_A}_{\text{degradation}} \quad (14)$$

where, for simplicity, the degradation of H_A is taken at a constant rate.

IL-1 β is secreted by healthy and infected M_2 , and this process is inhibited by I_α and I_{10} [17, 18, 20, 24]. Hence,

$$\frac{\partial I_{1\beta}}{\partial t} - D_{I_{1\beta}} \Delta I_{1\beta} = \underbrace{(\lambda_{I_{1\beta}M_2} M_2 + \lambda_{I_{1\beta}M_{2i}} M_{2i}) \frac{1}{1 + I_\alpha / \tilde{K}_\alpha} \frac{1}{1 + I_{10} / \tilde{K}_{10}}}_{\text{production}} - \underbrace{\mu_{I_{1\beta}} I_{1\beta}}_{\text{degradation}} \quad (15)$$

IL-2 is secreted by T_1 [17]; hence,

$$\frac{\partial I_2}{\partial t} - D_{I_2} \Delta I_2 = \underbrace{\lambda_{I_2 T_1} T_1}_{\text{production}} - \underbrace{\mu_{I_2} I_2}_{\text{degradation}} \quad (16)$$

IL-4 is secreted by T_1 , M_2 and M_{2i} [25, 26], so that the equation of I_4 is given by

$$\frac{\partial I_4}{\partial t} - D_{I_4} \Delta I_4 = \underbrace{(\lambda_{I_4 M_2} M_2 + \lambda_{I_4 M_{2i}} M_{2i} + \lambda_{I_4 T_2} T_2)}_{\text{production}} - \underbrace{\mu_{I_4} I_4}_{\text{degradation}} \quad (17)$$

IL-6 is produced by healthy and M_1 macrophages, a process enhanced by TNF- α [17–19]. Hence,

$$\frac{\partial I_6}{\partial t} - D_{I_6} \Delta I_6 = \underbrace{(\lambda_{I_6 M_1} M_1 + \lambda_{I_6 M_{1i}} M_{1i}) \left(1 + \frac{T_\alpha}{T_\alpha + K_{T_\alpha}}\right)}_{\text{production}} - \underbrace{\mu_{I_6} I_6}_{\text{degradation}} \quad (18)$$

IL-10 is produced by M_2 and M_{2i} [17–20], and by T_2 [27, 28]; so that

$$\frac{\partial I_{10}}{\partial t} - D_{I_{10}} \Delta I_{10} = \underbrace{(\lambda_{I_{10} M_2} M_2 + \lambda_{I_{10} M_{2i}} M_{2i} + \lambda_{I_{10} T_2} T_2)}_{\text{production}} - \underbrace{\mu_{I_{10}} I_{10}}_{\text{degradation}} \quad (19)$$

IL-12 is produced by M_1 and M_{1i} , a process inhibited by IL-10 and IL-13 [17, 20, 21]. Hence

$$\frac{\partial I_{12}}{\partial t} - D_{I_{12}} \Delta I_{12} = \underbrace{(\lambda_{I_{12} M_1} M_1 + \lambda_{I_{12} M_{1i}} M_{1i}) \frac{1}{1 + I_{10} / \tilde{K}_{10}} \frac{1}{1 + I_{13} / \tilde{K}_{13}}}_{\text{production}} - \underbrace{\mu_{I_{12}} I_{12}}_{\text{degradation}} \quad (20)$$

IL-13 is produced by M_2 and M_{2i} [17–20], and by T_2 [27–29]. Hence the equation of I_{13} is given as follows:

$$\frac{\partial I_{13}}{\partial t} - D_{I_{13}} \Delta I_{13} = \underbrace{(\lambda_{I_{13} M_2} M_2 + \lambda_{I_{13} M_{2i}} M_{2i} + \lambda_{I_{13} T_2} T_2)}_{\text{production}} - \underbrace{\mu_{I_{13}} I_{13}}_{\text{degradation}} \quad (21)$$

IFN- α is produced by T_1 and T_2 , a process resisted by IL-1 β [34], so that

$$\frac{\partial I_\alpha}{\partial t} - D_{I_\alpha} \Delta I_\alpha = \underbrace{(\lambda_{I_\alpha T_1} T_1 + \lambda_{I_\alpha T_2} T_2) \frac{1}{1 + I_{1\beta} / \tilde{K}_{1\beta}}}_{\text{production}} - \underbrace{\mu_{I_\alpha} I_\alpha}_{\text{degradation}} \quad (22)$$

IFN- γ is secreted by T_1 [17, 20, 35], a process resisted by IFN- α [23]. Hence IFN- γ satisfies the equation

$$\frac{\partial I_\gamma}{\partial t} - D_{I_\gamma} \Delta I_\gamma = \underbrace{\lambda_{I_\gamma T_1} \frac{1}{1 + I_\alpha / \tilde{K}_\alpha} T_1}_{\text{production}} - \underbrace{\mu_{I_\gamma} I_\gamma}_{\text{degradation}} \tag{23}$$

TNF- α is secreted by M_1, M_{1i} and M_{2i} , a process resisted by IL-10 [22] and IL-13 [23]. Hence the equation of T_α is given by

$$\frac{\partial T_\alpha}{\partial t} - D_{T_\alpha} \Delta T_\alpha = \underbrace{(\lambda_{T_\alpha M_1} M_1 + \lambda_{T_\alpha M_{1i}} M_{1i} + \lambda_{T_\alpha M_{2i}} M_{2i})}_{\text{production}} \frac{1}{1 + I_{10} / \tilde{K}_{10}} \frac{1}{1 + I_{13} / \tilde{K}_{13}} - \underbrace{\mu_{T_\alpha} T_\alpha}_{\text{degradation}} \tag{24}$$

TGF- β is produced by M_2 and M_{2i} , a process enhanced by IL-13 [30, 75]. Hence,

$$\frac{\partial T_\beta}{\partial t} - D_{T_\beta} \Delta T_\beta = \underbrace{(\lambda_{T_\beta M_2} M_2 + \lambda_{T_\beta M_{2i}} M_{2i})}_{\text{production}} \left(1 + \lambda_{T_\beta I_{13}} \frac{I_{13}}{I_{13} + K_{13}} \right) - \underbrace{\mu_{T_\beta} T_\beta}_{\text{degradation}} \tag{25}$$

MMP and TIMP are produced by M_2 and M_{2i} macrophages [31, 32], and depleted by binding to each other [73]. Hence the equations for M_p and T_p are given, respectively, as follows:

$$\frac{\partial M_p}{\partial t} - D_{M_p} \Delta M_p = \underbrace{\lambda_{M_p M_2} M_2 + \lambda_{M_p M_{2i}} M_{2i}}_{\text{production}} - \underbrace{d_{M_p T_p} T_p M_p}_{\text{depletion}} - \underbrace{\mu_{M_p} M_p}_{\text{degradation}} \tag{26}$$

$$\frac{\partial T_p}{\partial t} - D_{T_p} \Delta T_p = \underbrace{\lambda_{T_p M_2} M_2 + \lambda_{T_p M_{2i}} M_{2i}}_{\text{production}} - \underbrace{d_{T_p M_p} M_p T_p}_{\text{depletion}} - \underbrace{\mu_{T_p} T_p}_{\text{degradation}} \tag{27}$$

CCL3 is produced by infected M_1 and M_2 macrophages, as well as infected HSCs [45, 52, 53]. CCL3 is degraded naturally, but is also lost when internalized by M_1 [64]. Hence C_3 satisfies the equation:

$$\frac{\partial C_3}{\partial t} - D_{C_3} \Delta C_3 = \underbrace{\lambda_{C_3 H_i} H_i + \lambda_{C_3 M_{1i}} M_{1i} + \lambda_{C_3 M_{2i}} M_{2i}}_{\text{production}} - \underbrace{d_{C_3 M_1} \frac{C_3}{C_3 + K_{C_3}} M_1}_{\text{degradation}} - \mu_{C_3} C_3 \tag{28}$$

Equations for intracellular (V_{i1}, V_{i2}, V_{iH}) and extracellular (V_e) viruses. In order to explain the dynamics of the viral loads, we introduce the following notations: C will denote any of the cells M_1, M_2 or H , and C_i will denote their infected states. V_i will denote any of the intracellular viral loads V_{i1}, V_{i2} or V_{iH} . We assume that the growth rate of V_i is proportional to C_i , and is resisted by $I_\alpha, T_\alpha, T_\beta$ and I_γ , with the effect of I_γ being modulated by I_6 [20, 35, 55], thus reducing the growth rate coefficient λ by a factor $(1 + I_\alpha / \tilde{K}_\alpha)(1 + T_\alpha / \tilde{K}_{T_\alpha})(1 + T_\beta / \tilde{K}_{T_\beta})(1 + T_\gamma / (\tilde{K}_\gamma + I_6))$. There is also an increase of V_i at a rate proportional to $C V_e$ when external viruses are internalized by C cells [20]. We assume that the rate of this increase is $\lambda_{CC_i} N_V C V_e$, where N_V is a dimensionality coefficient which is of order of magnitude of (mass of 1 virus)/(mass of 1 cell). We assume that when one infected

cell, C_i , dies at rate $\mu_{C_i} = \mu_C(1 + \mu_{V_i} V_i)$, N viruses are released. We conclude that the density of intracellular viruses in C_i satisfies the equation

$$\frac{\partial V_i}{\partial t} - D_{C_i} \Delta V_i = \frac{\lambda C_i}{(1 + I_\alpha / \tilde{K}_\alpha)(1 + T_\alpha / \tilde{K}_{T_\alpha})(1 + T_\beta / \tilde{K}_{T_\beta})(1 + I_\gamma / (\tilde{K}_\gamma + I_6))} + \lambda_{C_i} N_V C V_e - \mu_{C_i} (1 + \mu_{V_i} V_i) N V_i.$$

Hence, we have the following equations for V_{i1} , V_{i2} , V_{iH} and V_e :

$$\begin{aligned} \frac{\partial V_{i1}}{\partial t} - D_M \Delta V_{i1} &= \underbrace{\frac{\lambda_{V_i M_{i1}} M_{i1}}{(1 + I_\alpha / \tilde{K}_\alpha)(1 + T_\alpha / \tilde{K}_{T_\alpha})(1 + T_\beta / \tilde{K}_{T_\beta})(1 + I_\gamma / (\tilde{K}_\gamma + I_6))(1 + A / \tilde{K}_A)}}_{\text{growth in } M_{i1}} \\ &+ \underbrace{\lambda_{M_{i1} M_{i1}} N_V M_{i1} V_e}_{V_e \rightarrow V_i} - \underbrace{\mu_{M_{i1}} (1 + \mu_{V_{i1}} V_{i1}) N V_{i1}}_{\text{death}} \end{aligned} \tag{29}$$

$$\begin{aligned} \frac{\partial V_{i2}}{\partial t} - D_M \Delta V_{i2} &= \underbrace{\frac{\lambda_{V_i M_{i2}} M_{i2}}{(1 + I_\alpha / \tilde{K}_\alpha)(1 + T_\alpha / \tilde{K}_{T_\alpha})(1 + T_\beta / \tilde{K}_{T_\beta})(1 + I_\gamma / (\tilde{K}_\gamma + I_6))(1 + A / \tilde{K}_A)}}_{\text{growth in } M_{i2}} \\ &+ \underbrace{\lambda_{M_{i2} M_{i2}} N_V M_{i2} V_e}_{V_e \rightarrow V_i} - \underbrace{\mu_{M_{i2}} (1 + \mu_{V_{i2}} V_{i2}) N V_{i2}}_{\text{death}} \end{aligned} \tag{30}$$

$$\begin{aligned} \frac{\partial V_{iH}}{\partial t} - D_H \Delta V_{iH} &= \underbrace{\frac{\lambda_{V_i H_i} H_i}{(1 + I_\alpha / \tilde{K}_\alpha)(1 + T_\alpha / \tilde{K}_{T_\alpha})(1 + T_\beta / \tilde{K}_{T_\beta})(1 + I_\gamma / (\tilde{K}_\gamma + I_6))(1 + A / \tilde{K}_A)}}_{\text{growth in } H_i} \\ &+ \underbrace{\lambda_{H H_i} N_V H V_e}_{V_e \rightarrow V_i} - \underbrace{\mu_H (1 + \mu_{V_{iH}} V_{iH}) N V_{iH}}_{\text{death}} \end{aligned} \tag{31}$$

Note that the diffusion coefficients of intracellular viruses were taken the same as the diffusion coefficients of their hosts. Note also that we have included the factor $\frac{1}{1+A/\tilde{K}_A}$ in the first terms on the right-hand sides of Eqs (29)–(31). This factor accounts for the control of the viral load within infected cells by a drug, such as adefovir, that inhibits the growth of the virus. If the drug is not given, then $A = 0$ and the factor $\frac{1}{1+A/\tilde{K}_A}$ may be dropped.

V_e is increased when infected cells die and release the virus that they contained. There is a reduction in V_e when cells internalize extracellular viruses and become infected. Hence,

$$\begin{aligned} \frac{\partial V_e}{\partial t} - D_{V_e} \Delta V_e &= \underbrace{N[\mu_{M_{i1}} (1 + \mu_{V_{i1}} V_{i1}) V_{i1} + \mu_{M_{i2}} (1 + \mu_{V_{i2}} V_{i2}) V_{i2} + \mu_H (1 + \mu_{V_{iH}} V_{iH}) V_{iH}]}_{\text{released by infected cells}} \\ &- \underbrace{(\lambda_{M_{i1} M_{i1}} M_{i1} + \lambda_{M_{i2} M_{i2}} M_{i2} + \lambda_{H H_i} H) N_V V_e}_{V_e \rightarrow V_i} - \underbrace{\mu_{V_e} V_e}_{\text{death}} \end{aligned} \tag{32}$$

Boundary Conditions. We simulate Model (1)–(32) in a rectangular domain Ω . We assume that the fibrosis occurs in Ω only, and hence we consider no-flux boundary conditions for all the variables.

Initial Conditions. We prescribe the following initial conditions in a unit of g/cm^3 :

$$\text{Cells: } M_1(0) = 3.48 \times 10^{-2}, M_{1i}(0) = 4.07 \times 10^{-3}, M_2(0) = 4.02 \times 10^{-2}, M_{2i}(0) = 4.86 \times 10^{-2}, H(0) = 4.97 \times 10^{-2}, H_i(0) = 2.67 \times 10^{-4}, T_1(0) = 9.44 \times 10^{-3}, T_2(0) = 3.01 \times 10^{-2}, f(0) = 6.2 \times 10^{-3}, m(0) = 3.31 \times 10^{-4};$$

$$\text{ECM: } \rho(0) = 2.7 \times 10^{-5};$$

$$\text{Cytokines and other proteins: } G(0) = 1.81 \times 10^{-11}, H_A(0) = 1.44 \times 10^{-6}, I_{1\beta}(0) = 5.5 \times 10^{-10}, I_2(0) = 1.47 \times 10^{-7}, I_4(0) = 2.3 \times 10^{-10}, I_6(0) = 1.29 \times 10^{-10}, I_{10}(0) = 2.2 \times 10^{-9}, I_{12}(0) = 4.19 \times 10^{-9}, I_{13}(0) = 3.53 \times 10^{-10}, I_\alpha(0) = 7.42 \times 10^{-10}, I_\gamma(0) = 1.77 \times 10^{-10}, T_\alpha(0) = 1.82 \times 10^{-10}, T_\beta(0) = 6.22 \times 10^{-7}, M_p(0) = 1.32 \times 10^{-5}, T_p(0) = 3.86 \times 10^{-7}, C_3(0) = 1.22 \times 10^{-10};$$

$$\text{HBV: } V_e(0) = 3.9 \times 10^{-12}, V_{i1}(0) = V_{i2}(0) = V_{iH}(0) = 1.6 \times 10^{-9}.$$

However, we note that the simulation results with different initial conditions do not appreciably change after a few days.

Results

All the computations are done using Python 2.7.6. The parameter values of the model equations are estimated in Section A in [S1 File](#) and are listed in Tables C–F in [S1 File](#). The techniques used for the simulations are also described in Section B in [S1 File](#).

[Fig 2](#) is a simulation of the averages of the model variables for 180 days. We see that most of the variables are not in steady state, in agreement with the progressive state of HBV in chronic stage. The densities of uninfected phagocytic cells (M_1 , M_2 and H) decrease while the densities of the infected phagocytic cells (M_{1i} , M_{2i} and H_i) increase. The increase in the densities of infected phagocytic cells results in an increase of the inflammation as seen in the profiles of IFN- γ and TNF- α , in agreement with chronic HBV progression. While M_2 decreases and M_{2i} increases, the production term $\lambda_{M_p, M_2} M_2 + \lambda_{M_p, M_{2i}} M_{2i}$ of M_p increases, as seen in the increasing profile of M_p . The simulations show that the densities of both Th1 cells and Th2 cells increase, while the Th2 cells are dominant. The increase in IL-10 and decrease in IL-12 suggest that the immune system is not strong enough to confront the infection. Cytokines produced by Th1 cells tend to reduce the load of intracellular viruses, while cytokines produced by Th2 cells work in the opposite direction. It is therefore interesting to note that, since T_2 dominates T_1 , the viral loads (mostly represented by the intracellular HBV) are continuously increasing. Our model also shows that the density of fibroblasts decreases monotonically while the density of myofibroblasts increases, which enhances the production of ECM; the transition from fibroblast to myofibroblast is induced by PDGF and TGF- β , and it increases in time. The concentrations of MMP and TIMP also increase in time. The scar continues to grow, as a result of the increase in MMP and ECM.

We can also simulate the spatial variations of the variables, however we are interested, in this paper, only in the average profiles of the variables. One is tempted to use the simpler ODE model to compute averages. We note however that the diffusion coefficients of cytokines and extracellular viruses are several orders of magnitude larger than the diffusion coefficients of cells. For this reason the ODE system cannot adequately represent the spread of the infection, and hence, the averages of the variables. Indeed, in the simulation of the ODE system (not shown here) the infected macrophages decrease, rather than increase; healthy HSCs are increasing, rather than decreasing, and the intracellular and extracellular viruses decrease and stabilize, rather than monotonically increase, as in [Fig 2](#).

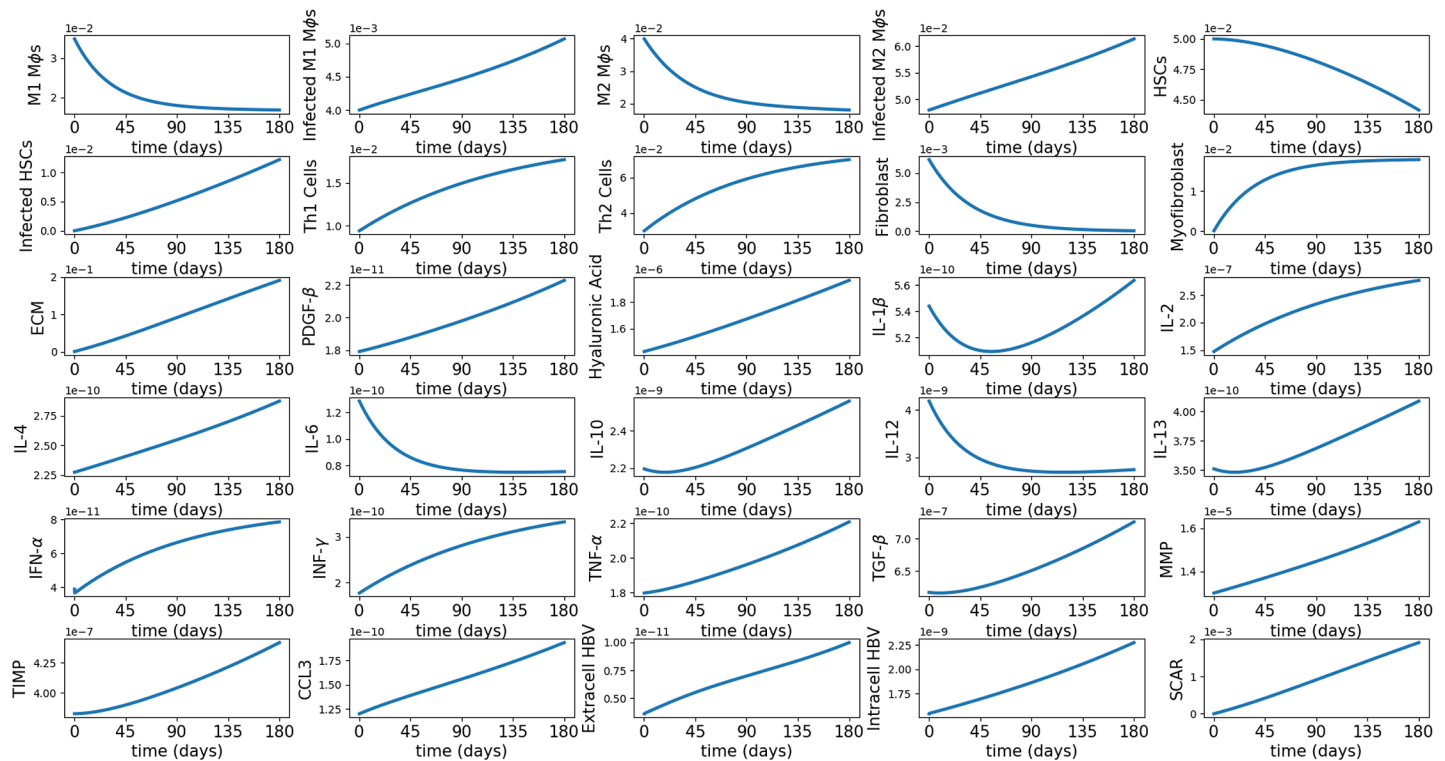


Fig 2. Simulation of all the average densities/concentrations of the variables for Model (1)–(28) over a period of 180 days.

<https://doi.org/10.1371/journal.pone.0195037.g002>

Treatment

In this section, we consider two drugs that are commonly used for the treatment of HBV, namely IFN- α and adefovir [5, 6, 12, 13]. Treatment with IFN- α in chronic HBV adult patient ranges between 16–52 weeks, while treatment with adefovir is continuous for 2–3 years [39, 76]. In oncology, it is found that in case of intermittent therapies in which the drug amount administered per unit time is constant, the response is significantly influenced by the amount of drug given and the period of time within which the drug is given [77–79]. Moreover, if negative side effects are ignored, then by doubling the amount of drug and correspondingly shortening the period of treatment (keeping the total amount of drug fixed) we may get better results in reducing the infection [65]. Assuming that the total amount of each drug is fixed, we use the mathematical model to evaluate the efficacy of combination therapy with IFN- α and adefovir. We start the treatment after 90 days of control and administer the drugs for 90 days.

Treatment with IFN- α . In our model, injection of IFN- α is represented as a source term, $c_\alpha(t)$, in Eq (22), which then takes the form

$$\frac{\partial I_\alpha}{\partial t} - D_{I_\alpha} \Delta I_\alpha = \underbrace{c_\alpha(t)}_{\text{source term}} + \underbrace{\lambda_{I_\alpha T_1} T_1 + \lambda_{I_\alpha T_2} M_{2i} \frac{1}{1 + I_{1\beta}/\tilde{K}_{1\beta}}}_{\text{production}} - \underbrace{\mu_{I_\alpha} I_\alpha}_{\text{degradation}}. \quad (33)$$

Treatment with adefovir (A). We denote the source of the drug by $c_A(t)$. The drug is diminished by absorption by infected cells, and by natural degradation. Hence, the equation of

adefovir, A , is given by

$$\frac{\partial A}{\partial t} - D_A \Delta A = \underbrace{c_A(t)}_{\text{source}} - \underbrace{(\lambda_{M_{1i}A} M_{1i} + \lambda_{M_{2i}A} M_{2i} + \lambda_{H_iA} H_i)}_{\text{absorption}} \frac{A}{A + K_A} - \underbrace{\mu_A A}_{\text{degradation}}. \tag{34}$$

Combination therapy with IFN- α and adefovir. Combination therapy with IFN- α and adefovir is modeled by using Eqs (33) and (34) together with System (1)–(32). Adefovir is given daily in one or two tablets [80], and its effective time is about 10 hours [81]. For simplicity, we assume a daily average constant level c_A taking

$$c_A = \begin{cases} 10^{-4} \text{ g/cm}^3 \text{ d}^{-1}, & 90 < t < 180; \\ 0, & \text{elsewhere.} \end{cases} \tag{35}$$

IFN- α is given in shots three times a week, or in slow injection, as pegylated IFN- α , once a week [82]. We assume that it is given once a week at level c_α , so that after t days its level reduces to

$$c_\alpha e^{-\sigma t}, \quad \text{for some } \sigma > 0,$$

and at the end of the week ($t = 7$ days) its level is negligible, taking

$$c_\alpha e^{-7\sigma} = \frac{1}{X} c_\alpha, \quad X = e^7,$$

so that $\sigma = 1$. The average level during the week is

$$\frac{1}{7} \int_0^7 c_\alpha e^{-t} dt = \frac{c_\alpha}{7} (1 - e^{-7}) \sim \frac{c_\alpha}{7}.$$

We wish to simplify the simulations by replacing the intermittent treatment of injections at level $7c_\alpha$ by a constant level of the drug at the level c_α , that is, by

$$c_\alpha(t) = \begin{cases} 10^{-7} \text{ g/cm}^3 \text{ d}^{-1}, & 90 < t < 180; \\ 0, & \text{elsewhere.} \end{cases} \tag{36}$$

In order to justify this simplification, we simulated in Figs 3 and 4 the average densities of all the variables with treatment (IFN- α –orange, adefovir–green and combination–red) and without treatment when the drugs are given intermittently (Fig 3) and continuously (Fig 4).

We see that the profiles of the virus and scar are almost the same under Figs 3 and 4. Hence, for simplicity, we shall use the scheme for Fig 4, that is, Eqs (35) and (36), to compute the efficacy and synergy maps.

Therapy with continuous drug delivery. From Fig 4, we see that IFN- α reduces the viral load by 30.36%, which agrees with reported clinical results by Paul and Han [83]; adefovir reduces by 42.28% and the combination reduces by 57.66%. The reduction in the scar is 20.41% by IFN- α , 28.24% by adefovir, and 37.8% by the combination, although the scar still keeps increasing. We also see that the drugs (in monotherapy and in combination therapy) effectively reduce the inflammation by considerably reducing the densities of infected phagocytic cells (M_{1i} , M_{2i} and H_i), and the pro-inflammatory cytokine TNF- α . The pro-inflammatory cytokines IL-6 and IL-12 already have decreasing profiles in the control case, making the effect of drugs on them less significant. We observe in Fig 4 that the drugs have little (or no)

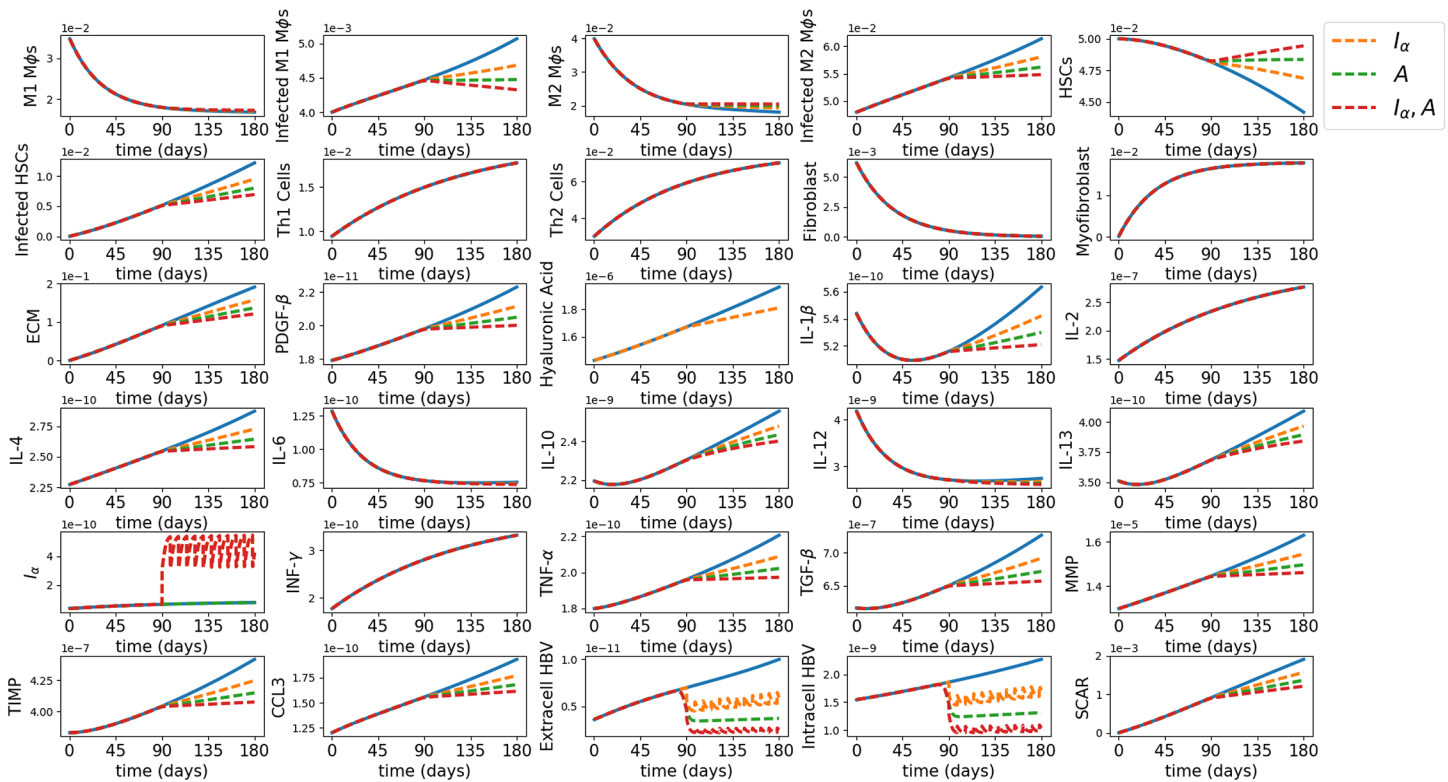


Fig 3. Monotherapy and combination therapy with intermittent IFN- α and continuous adefovir. The horizontal axes scale the time in days and the vertical axes scale the average densities in g/cm^3 for all the variables for the first 180 days since the start of the disease, in control case (blue) and with treatment (IFN- α –orange, adefovir–blue and combination–red).

<https://doi.org/10.1371/journal.pone.0195037.g003>

effect on the profiles of Th1 and Th2 cells, and hence also on IFN- γ and IL-2 which are secreted by T cells.

We proceed to consider the effect of therapy for a range of doses of adefovir and IFN- α . We denote by $S_X(180)$ and $V_{i,X}(180)$ the densities of S and V_i , respectively, at day 180 under administration of drug X , where X is either adefovir alone, or IFN- α alone, or their combination. We denote by $S(180)$ and $V_i(180)$ the densities of S and V_i , respectively, at day 180 in the control case (no drugs), and define two efficacy functions:

$$E_S(X) = \frac{S(180) - S_X(180)}{S(180)} \times (100\%)$$

$$E_{V_i}(X) = \frac{V_i(180) - V_{i,X}(180)}{V_i(180)} \times (100\%).$$
(37)

Fig 5A is an efficacy map for the scar density under the combined therapy with $X = (c_A, c_\alpha)$, and Fig 5B is the corresponding efficacy map for the viral load V_i ; the color columns colors show the efficacy values.

Both IFN- α and adefovir can have severe side-effects when administered alone. These side-effects could be aggravated if both drugs are given simultaneously with the same doses as in monotherapy. Thus, there is the need to find a strategy for combination therapy that maximizes the efficacy while reducing the sides effects. The dose-response relationship of the

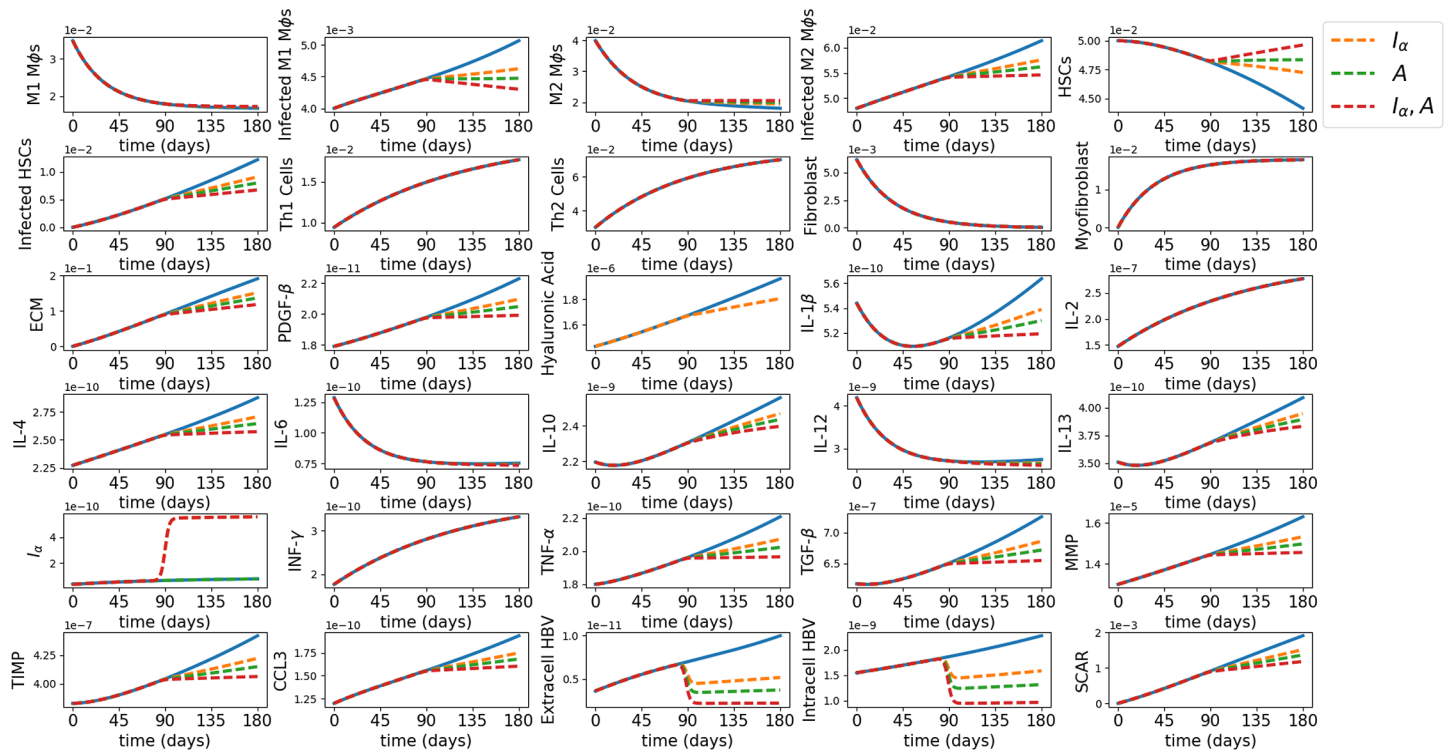


Fig 4. Monotherapy and combination therapy with IFN- α and adefovir. The horizontal axes scale the time in days and the vertical axes scale the average densities in g/cm^3 for all the variables for the first 180 days since the start of the disease, in control case (blue) and with treatment (IFN- α –orange, adefovir–blue and combination–red).

<https://doi.org/10.1371/journal.pone.0195037.g004>

amount of drugs to the severity of negative side-effects has been extensively studied [84–86]: at higher doses, undesired side-effects appear and grow stronger with increases in the dose.

We compare treatment of combination therapy (c_{α}, c_A) with monotherapy I_{α} and monotherapy A . For monotherapy I_{α} we take $(1 + \theta_{I_{\alpha}})c_{\alpha}$ and for monotherapy A we take $(1 + \theta_A)c_A$, with $\theta_{I_{\alpha}} > 0, \theta_A > 0$, to reflect the highest toxicity expected when combining the two drugs. If $E_S(c_{\alpha}, c_A)$ is larger than both $E_S((1 + \theta_{I_{\alpha}})c_{\alpha}, 0)$ and $E_S(0, (1 + \theta_A)c_A)$, then we say that the ‘synergy’ in scar density reduction for the combination (c_{α}, c_A) is positive, and otherwise, we say that the synergy is negative [87]. Similarly, if $E_{V_i}(c_{\alpha}, c_A)$ is larger than both $E_{V_i}((1 + \theta_{I_{\alpha}})c_{\alpha}, 0)$ and $E_{V_i}(0, (1 + \theta_A)c_A)$, then we say that the synergy in viral load reduction for the combination (c_{α}, c_A) is positive, and otherwise, we say that the synergy is negative [87]. More generally, we define the synergy in scar density reduction $\sigma_S = \sigma_S(c_{\alpha}, c_A)$ by the formula (as in [87]):

$$\sigma_S(c_{\alpha}, c_A) = \frac{E_S(c_{\alpha}, c_A)}{\max\{E_S((1 + \theta_{I_{\alpha}})c_{\alpha}, 0), E_S(0, (1 + \theta_A)c_A)\}} - 1. \tag{38}$$

Then $\sigma_S(c_{\alpha}, c_A) > 0$ (positive synergy) if the combination (c_{α}, c_A) reduces the level of scar density more than either one of the single agents $(1 + \theta_{I_{\alpha}})c_{\alpha}$ or $(1 + \theta_A)c_A$. Negative synergy occurs in the reverse case where instead of a combination therapy with (c_{α}, c_A) we achieve better reduction of the level of scar density if we apply only one drug, $(1 + \theta_{I_{\alpha}})c_{\alpha}$ or $(1 + \theta_A)c_A$. Similarly we

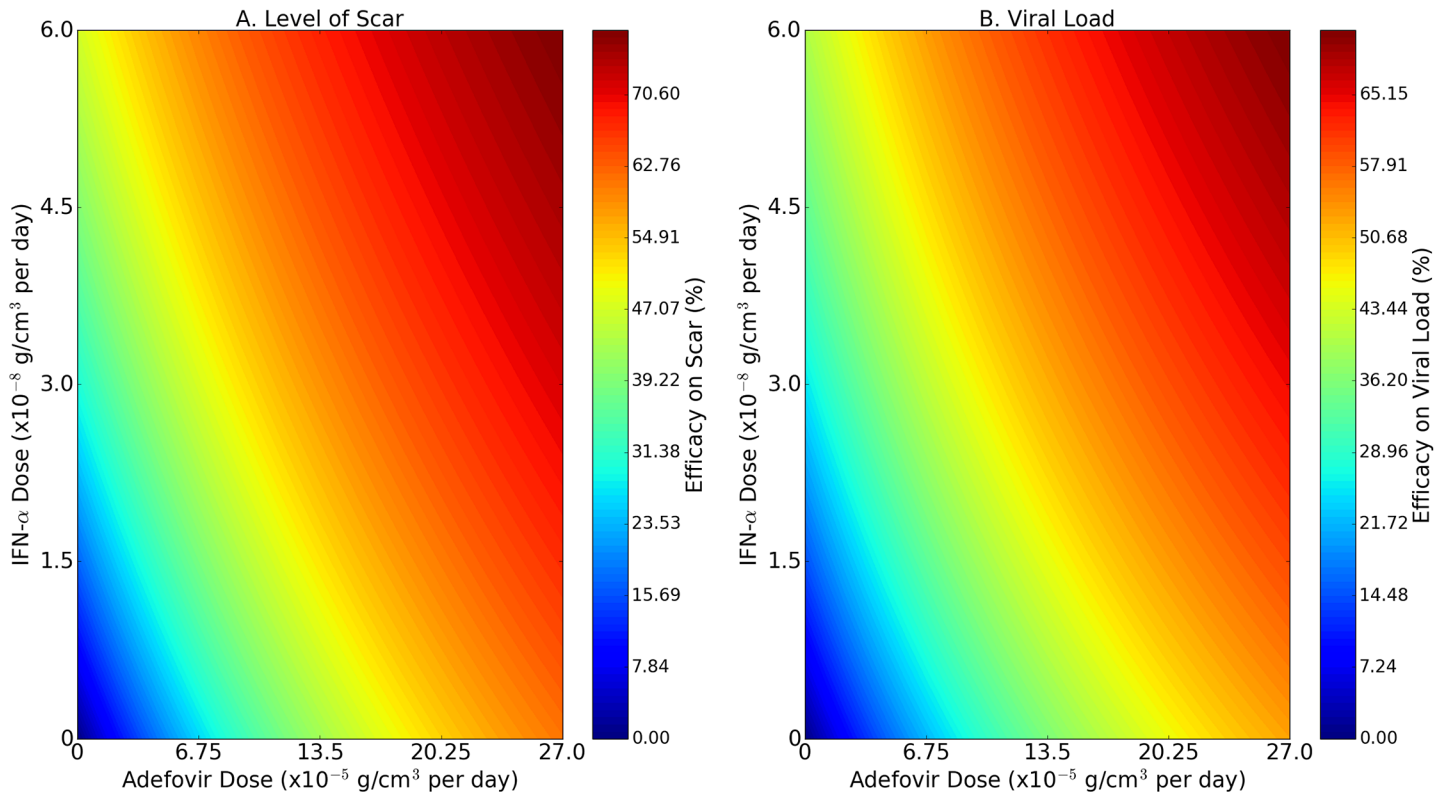


Fig 5. Efficacy map in combination therapy with IFN- α and adefovir. The horizontal axes scale the fractions for the dose of IFN- α and the vertical axes scale the fractions for the dose of adefovir. The color maps represent the efficacies of reduction in the level of scar density (A) and the viral load (B) at day 180 of infection.

<https://doi.org/10.1371/journal.pone.0195037.g005>

define the synergy in reducing the viral load by the formula:

$$\sigma_{V_i}(c_z, c_A) = \frac{E_{V_i}(c_z, c_A)}{\max\{E_{V_i}((1 + \theta_{I_\alpha})c_z, 0), E_{V_i}(0, (1 + \theta_A)c_A)\}} - 1. \tag{39}$$

There are negative side-effects such as lactic acidosis in the case of treatment with adefovir, and serious depression in the case of IFN- α [88]. Since the mechanisms of these side-effects are not well understood, and since it is difficult to evaluate and compare the severity of these side-effects, we take for definiteness $\theta_{I_\alpha} = \theta_A = 2$; this choice is arbitrary and could be made more precise as more clinical data become available that will inform on the side-effects associated with IFN- α and adefovir, separately or in combination.

Fig 6 shows the ‘synergy map’ associated with Model (1)–(32) where we compute the values for the synergy as in Eq (38) related with the drugs IFN- α (I_α) and adefovir (A). The color columns assign a “synergy number” (SN) to any level of adefovir and IFN- α ; SN varies from -0.16 to 0.64 for the level of scar density, and from -0.15 to 0.69 for the viral load. Given any level of c_ω , as c_A initially increases so does the SN, until c_A reaches a level c_A^* which depends on c_ω ; i.e., $c_A^* = c_A(c_\omega)$. Thereafter, the SN begins to decrease as c_A increases. The biological explanation of the color patterns in the synergy maps can be traced to the fact that the virus proliferation is inhibited by the product $(1 + I_\alpha/\tilde{K}_\alpha)(1 + A/\tilde{K}_A)$, as seen in Eqs (29)–(31). This product is highly correlated, after scaling, to the product $(1 + c_\omega)(1 + c_A)$. Viewing this product

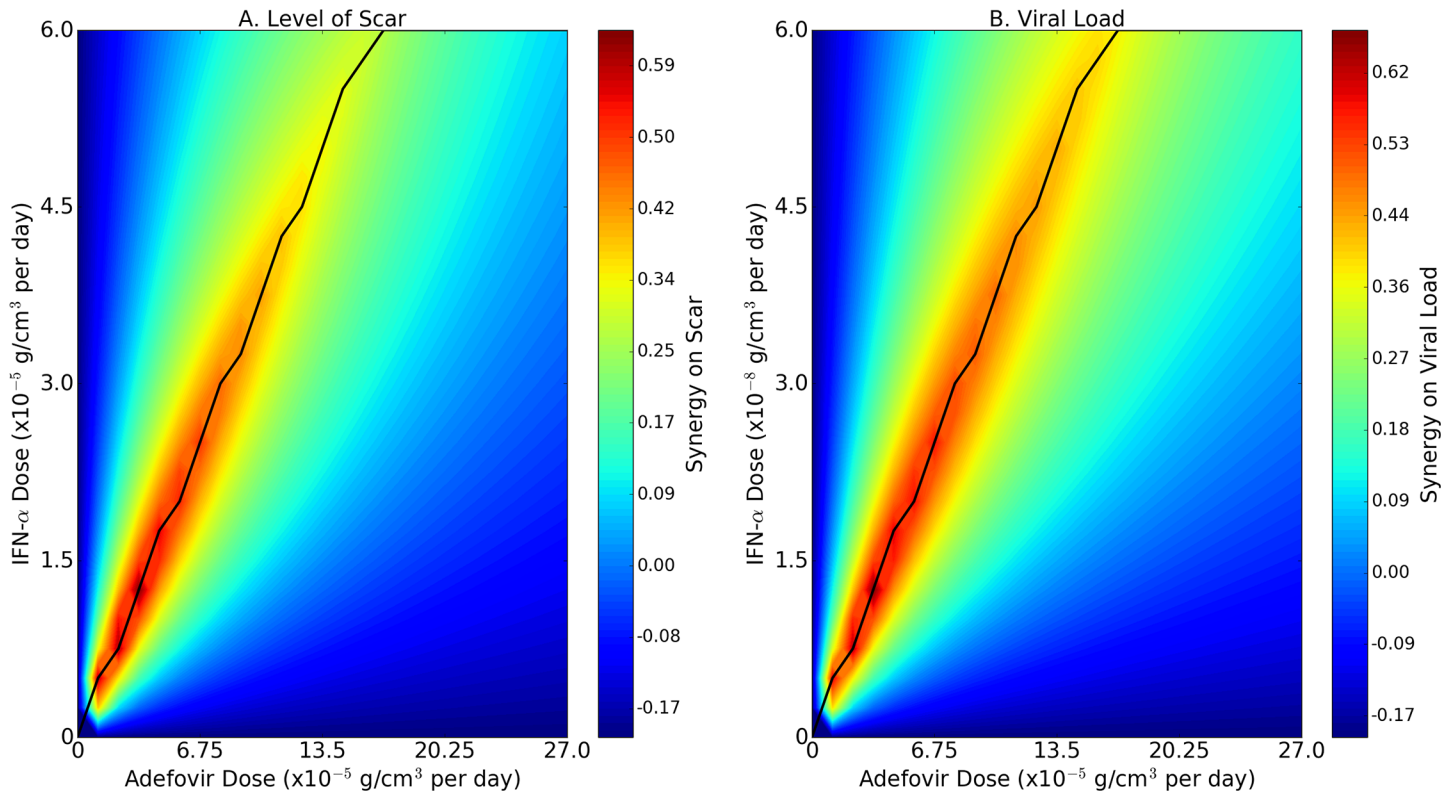


Fig 6. Synergy map for drugs IFN- α and adefovir in HBV. The horizontal axes scale the dose of IFN- α and the vertical axes scale the dose of adefovir. The color maps represent the synergies between the two drugs IFN- α and adefovir in reducing the level of scar density (A) and the viral load (B) at day 180 of infection.

<https://doi.org/10.1371/journal.pone.0195037.g006>

as representing the efficacy of the combined therapy, the resulting expression for the synergy is then a function of the following type:

$$f(c_\alpha, c_A) = \frac{(1 + c_\alpha)(1 + c_A)}{\max(1 + 3c_\alpha, 1 + 3c_A)} - \text{constant}.$$

We now observe that $f(c_\alpha, c_A)$ is an increasing function in c_A if $c_A < c_\alpha$ and a decreasing function in c_A if $c_A > c_\alpha$, and similarly, $f(c_\alpha, c_A)$ is increasing in c_α if $c_\alpha < c_A$ and is decreasing in c_α if $c_\alpha > c_A$; and this behavior is reflected in the synergy maps. In both synergy maps Fig 6A and 6B, SN is negative when $c_A < 1.25 \times 10^{-5}$ g/cm³ per day, or $c_\alpha < 0.15 \times 10^{-8}$ g/cm³ per day. Negative synergy indicates that it is more beneficial to use monotherapy with either $3c_\alpha$ or $3c_A$ instead of combination therapy with (c_α, c_A) . However this conclusion does not take into account negative side-effects.

Discussion

Hepatitis B virus (HBV) infection is one of the most prevalent infectious diseases associated with human liver. Despite the availability of a vaccine, HBV remains a global health problem, which affects more than 350 million people annually, with 600,000 deaths resulting from HBV-related liver diseases. One of the hallmarks of the disease is the development of liver fibrosis. Anti-HBV drugs currently in use include adefovir, which is anti-viral therapy, and IFN- α , which decreases viremia, inflammation and liver fibrosis. The treatment with each of

these drugs typically extends over a period of many months, and incurs severe negative side-effects; kidney damage, low amount of phosphate in the blood, stroke and pancreatitis for adefovir, brain disorder, heart attack and lung fibrosis for IFN- α .

In the present paper, we considered the effect of these two drugs on slowing the growth of liver fibrosis associated with HBV. With the aim of using the least amount of drugs, we asked the following question: Is a combination of adefovir and IFN- α at a certain level more effective in reducing the fibrotic scar than a monotherapy with either adefovir or IFN- α at an ‘appropriate’ increased level? If so, we say that the combination therapy is *synergetic*. We developed a mathematical model by a system of PDEs and used the model to address this question. The model includes cells and cytokines that significantly affect the fibrosis of the liver in HBV. Some of the parameters were taken from the literature, while others were estimated under some assumptions; simulations of the model validated these assumptions.

The main result of the paper is the “synergy maps” in Fig 6. The color columns assign a “synergy numbers” (SN) to any level of adefovir (c_A) and IFN- α (c_α). Given any level of c_α as c_A initially increases so does each SN, until c_A reaches a level c_A^* which depends on c_α ; i.e., $c_A^* = c_\alpha(c_A)$. Thereafter, the SN begins to decrease as A increases. We suggest that the dosage of IFN- α should be related to adefovir so that the proportion should lie as closed as possible to both solid curves in Fig 6.

In Fig 6, negative synergy means that it is more beneficial to treat the patient with either IFN- α or adefovir as a single agent, rather than with combination of the two drugs. In the definition of efficacy we compared treatment of combination therapy (c_α, c_A) to monotherapy with either $(1 + \theta_{I_\alpha})c_\alpha$ or $(1 + \theta_A)c_A$, where we took $\theta_{I_\alpha} = \theta_A = 2$. This choice was quite arbitrary. If it turns out that the negative side-effects in the combined therapy are much more severe than the negative side-effects of a monotherapy with either IFN- α and adefovir, then it would be more appropriate to increase the values of θ_A and θ_{I_α} in the synergy map. On the other hand, if the negative side-effects from the combination are not significantly more severe than the negative side-effects from either one of the two drugs, then it would be appropriate to decrease the chosen values of θ_A and θ_{I_α} in the synergy map. A meta-analysis for the comparison of efficacy in the combination IFN- α -adefovir versus IFN- α in monotherapy is done in [89]. In this work that does not include the effect of drug toxicity, the authors show that the efficacy of IFN- α plus adefovir combination therapy is superior to IFN- α monotherapy. However, combined clinical data on efficacy and toxicity are quite limited at this time. Hence, our model should be viewed as setting up a computational framework, to address the question of optimal efficacy in combination therapy with IFN- α and adefovir.

Supporting information

S1 File. Supporting information—Chronic hepatitis B virus and liver fibrosis: A mathematical model. Parameter estimates (Section A in S1 File), parameter values (Tables C–F in S1 File) and numerical methods used (Section B in S1 File).
(PDF)

Acknowledgments

This research was supported by the Mathematical Biosciences Institute of The Ohio State University. This work was conducted while Nourridine Siewe was a Postdoctoral Fellow at the National Institute for Mathematical and Biological Synthesis, an Institute sponsored by the National Science Foundation through NSF Award #DBI-1300426, with additional support from The University of Tennessee, Knoxville.

Author Contributions

Conceptualization: Avner Friedman, Nourridine Siewe.

Formal analysis: Avner Friedman, Nourridine Siewe.

Funding acquisition: Avner Friedman, Nourridine Siewe.

Methodology: Avner Friedman, Nourridine Siewe.

Project administration: Avner Friedman, Nourridine Siewe.

Resources: Avner Friedman, Nourridine Siewe.

Software: Nourridine Siewe.

Validation: Avner Friedman, Nourridine Siewe.

Writing – original draft: Avner Friedman, Nourridine Siewe.

Writing – review & editing: Avner Friedman, Nourridine Siewe.

References

1. Inuzuka T, Takahashi K, Chiba T, Marusawa H. Mouse models of hepatitis B virus infection comprising host-virus immunologic interactions. *Pathogens*. 2014; 3:377–389. <https://doi.org/10.3390/pathogens3020377> PMID: 25437805
2. Ott JJ, Stevens GA, Groeger J, Wiersma S. Global epidemiology of hepatitis B virus infection: new estimates of age-specific HBsAg seroprevalence and endemicity. *Vaccine*. 2012; 30(12):2212–2219. <https://doi.org/10.1016/j.vaccine.2011.12.116> PMID: 22273662
3. Schweitzer A, Horn J, Mikolajczyk RT, et al. Estimations of worldwide prevalence of chronic hepatitis B virus infection: a systematic review of data published between 1965 and 2013. *Lancet*. 2015 October; 386(10003):1546–1555. [https://doi.org/10.1016/S0140-6736\(15\)61412-X](https://doi.org/10.1016/S0140-6736(15)61412-X) PMID: 26231459
4. Tzeng H, Tsai H, Liao H, Chen C, Chen P, Hsu P. Tumor necrosis factor-alpha induced by hepatitis B virus core mediating the immune response for hepatitis B viral clearance in mice model. *PLoS ONE*. 2014 July; 9(7):1–8. <https://doi.org/10.1371/journal.pone.0103008>
5. Song J, Zhou Y, Li S, Wang B, Zheng X, Wu J, et al. Susceptibility of different hepatitis B virus isolates to interferon-alpha in a mouse model based on hydrodynamic injection. *PLoS ONE*. 2014 March; 9(3):1–9. <https://doi.org/10.1371/journal.pone.0090977>
6. Byrnes AA, Li DY, Park K, Thompson D, Mociłnikar C, Mohan P, et al. Modulation of the IL-12/IFN- γ axis by IFN- α therapy for hepatitis C. *J Leuc Biol*. 2007 March; 81:825–834. <https://doi.org/10.1189/jlb.1006622>
7. Asselah T, Lada O, Roucani M, Martinot M, Boyer N, Marcellin P. Interferon therapy for chronic hepatitis B. *Clin Liver Dis*. 2007; 11:839–849. <https://doi.org/10.1016/j.cld.2007.08.010> PMID: 17981231
8. Liu Y, Wu T, Sun N, Wang G, Yuan J, Dai Y, et al. Combination therapy with pegylated interferon alpha-2b and adefovir dipivoxil in HBsAg-positive chronic hepatitis B versus interferon alone: a prospective, randomized study. *J Huazhong Univ Sci Technol*. 2014; 34(4):542–547. <https://doi.org/10.1007/s11596-014-1312-2>
9. Loggi E, Vitale G, Conti F, Bernardi M, Andreone P. Chronic hepatitis B: Are we close to a cure? *Digestive and Liver Disease*. 2015 October; 47(10):836–841. <https://doi.org/10.1016/j.dld.2015.05.019> PMID: 26138799
10. Ebert G, Preston S, Allison C, Cooney J, Toe JG, Stutz MD, et al. Cellular inhibitor of apoptosis proteins prevent clearance of hepatitis B virus. *PNAS*. 2015 May 5; 112(18):5797–5802. <https://doi.org/10.1073/pnas.1502390112> PMID: 25902529
11. Ebert G, Allison C, Preston S, Cooney J, Toe JG, Stutz MD, et al. Eliminating hepatitis B by antagonizing cellular inhibitors of apoptosis. *PNAS*. 2015 May 5; 112(18):5803–5808. <https://doi.org/10.1073/pnas.1502400112> PMID: 25902530
12. Manolakopoulos S, Bethanis S, Koutsounas S, Goulis J, Vlachogiannakos J, Christias E, et al. Long-term therapy with adefovir dipivoxil in hepatitis B e antigen-negative patients developing resistance to lamivudine. *Aliment Pharmacol Ther*. 2008 February; 27(3):266–273. <https://doi.org/10.1111/j.1365-2036.2007.03567.x> PMID: 17988233

13. Marcellin P, Chang TT, Lim SG, Sievert MJTW, Shiffman ML, Jeffers L, et al. Adefovir dipivoxil for the treatment of hepatitis B e antigen-positive chronic hepatitis B. *N Engl J Med*. 2003 February; 348(9):808–816. <https://doi.org/10.1056/NEJMoa020681> PMID: 12606735
14. WedMD, LLC. List interferon alfa-2b injection side effects by likelihood and severity. *Side Effects*. 2017;.
15. WedMD, LLC. List adefovir side effects by likelihood and severity. *Side Effects*. 2017;.
16. Bility MT, Chiang L, Zhang Z, Luan Y, Li F, Chi L, et al. Hepatitis B Virus Infection and Immunopathogenesis in a Humanized Mouse Model: Induction of Human-Specific Liver Fibrosis and M2–Like Macrophages. *PLOS Pathogens*. 2014 March; 10(3):1–14. <https://doi.org/10.1371/journal.ppat.1004032>
17. Akdis M, Burgler S, Cramer R, Eiwegger T, Fujita H, Gomez E, et al. Interleukins, from 1 to 37, and interferon- γ : Receptors, functions, and roles in diseases. *J Allergy Clin Immunol*. 2011 March; (127):701–721. <https://doi.org/10.1016/j.jaci.2010.11.050> PMID: 21377040
18. Boltjes A, Movita D, Boonstra A, Woltman AM. The role of Kupffer cells in hepatitis B and hepatitis C virus infections. *Journal of Hepatology*. 2014; 61:660–671. <https://doi.org/10.1016/j.jhep.2014.04.026> PMID: 24798624
19. Liu H, Zhang X. Innate immune recognition of hepatitis B virus. *World J Gastroenterol*. 2015; 7(21):2319–2322.
20. Phillips S, Chokshi S, Riva A, Evans A, Williams R, Naoumov NV. CD8⁺ T cell control of hepatitis B virus replication: Direct comparison between cytolytic and noncytolytic functions. *J Immunol*. 2010; 184:287–295. <https://doi.org/10.4049/jimmunol.0902761> PMID: 19949099
21. Poovorawan K, Tangkijvanich P, Chirathaworn C, Wisedopas N, Treeprasertsuk S, Komolmit P, et al. Circulating cytokines and histological liver damage in chronic hepatitis B infection. *Hepatitis Research and Treatment*. 2013; 2013(757246):1–7. <https://doi.org/10.1155/2013/757246>
22. Oswald IP, Wynn TA, Sher A, James SL. Interleukin 10 inhibits macrophage microbicidal activity by blocking the endogenous production of tumor necrosis factor alpha required as a costimulatory factor for interferon gamma-induced activation. *Proc Natl Acad Sci USA*. 1992; 89(18):8676–8680. <https://doi.org/10.1073/pnas.89.18.8676> PMID: 1528880
23. Mayer-Baker KD, Andrade BB, otand SD, Amaral EP, Barber DL. Host-directed therapy of tuberculosis based on interleukin-1 and type I interferon crosstalk. *Nature*. 2014; 511(7507):99–103. <https://doi.org/10.1038/nature13489>
24. Senoo H. Structure and function of hepatic stellate cells. *Med Electron Microsc*. 2004 March; 37(1):3–15. <https://doi.org/10.1007/s00795-003-0230-3> PMID: 15057600
25. Buttner C, Skupin A, Reimann T, Rieber EP, Unteregger G, Geyer P, et al. Local production of interleukin-4 during radiation-induced pneumonitis and pulmonary fibrosis in rats: macrophages as a prominent source of interleukin-4. *Am J Respir Cell Mol Biol*. 1997; 17(3):315–325. <https://doi.org/10.1165/ajrcmb.17.3.2279> PMID: 9308918
26. Pouliot P, Turmel V, Gelinas E, Laviolette M, Bissonette EY. Interleukin-4 production by human alveolar macrophages. *Clin Exp Allergy*. 2005; 35(6):804–810. <https://doi.org/10.1111/j.1365-2222.2005.02246.x> PMID: 15969673
27. Jiang Y, Ma Z, Xin G, Yan H, Li W, Xu H, et al. Th1 and Th2 Immune Response in Chronic Hepatitis B Patients during a Long-Term Treatment with Adefovir Dipivoxil. *Mediators Inflamm*. 2010; 2010:1–10. <https://doi.org/10.1155/2010/143026>
28. Viallard JF, Pellegrin JL, Schaeverbeke T, Dehais J, Longy-Boursier M, Ragnaud JM, et al. Th1 (IL-2, interferon-gamma (IFN- γ)) and Th2 (IL-10, IL-4) cytokine production by peripheral blood mononuclear cells (PBMC) from patients with systemic lupus erythematosus (SLE). *Clin Exp Immunol*. 1999 January; 115(1):189–195. <https://doi.org/10.1046/j.1365-2249.1999.00766.x> PMID: 9933441
29. Venkayya R, Lam M, Willkom M, Grunig G, Corry DB, Erle DJ. The Th2 lymphocyte products IL-4 and IL-13 rapidly induce airway hyperresponsiveness through direct effects on resident airway cells. *Am J Respir Cell Mol Biol*. 2002 October; 26(2):202–208. <https://doi.org/10.1165/ajrcmb.26.2.4600> PMID: 11804871
30. Fichtner-Feigl S, Strober W, Kawakami K, Puri RK, Kitani A. IL-13 signaling through the IL-13 α 2 receptor is involved in induction of TGF- β 1 production and fibrosis. *Nat Med*. 2006; 12:99–106. <https://doi.org/10.1038/nm1332> PMID: 16327802
31. Vernon MA, Mylonas KJ, Hughes J. Macrophages and renal fibrosis. *Semin Nephrol*. 2010; 30:302–317. <https://doi.org/10.1016/j.semnephrol.2010.03.004> PMID: 20620674
32. Zhao H, Dong Y, Tian X, Tan TK, Liu Z, Zhao Y, et al. Matrix metalloproteinases contribute to kidney fibrosis in chronic kidney diseases. *World J Nephrol*. 2013; 2:84–89. <https://doi.org/10.5527/wjn.v2.i3.84> PMID: 24255890

33. Janeway CA, Travers P, Walport M, Schlomchik MJ. Immunobiology: The Immune System in Health and Disease. 2nd ed.; 2001.
34. Klimpel GR, Infante AJ, Patterson J, Hess CB, Asuncion M. Virus-induced interferon alpha/beta (IFN-alpha/beta) production by T cells and by Th1 and Th2 helper T cell clones: a study of the immunoregulatory actions of IFN-gamma versus IFN-alpha/beta on functions of different T cell populations. *Cell Immunol.* 1990 July; 128(2):603–618. [https://doi.org/10.1016/0008-8749\(90\)90052-S](https://doi.org/10.1016/0008-8749(90)90052-S) PMID: 2162739
35. Balmasova IP, Yushchuk ND, Mynbaev OA, Alla NR, Malova ES, Shi Z, et al. Immunopathogenesis of chronic hepatitis B. *World J Gastroenterol.* 2014 October 21; 20(39):14156–14171. <https://doi.org/10.3748/wjg.v20.i39.14156> PMID: 25339804
36. Yates A, Callard R, Stark J. Combining cytokine signaling with T-bet and GATA-3 regulation in Th1 and Th2 differentiation: A model for cellular decision-making. *J Theo Biol.* 2004; 231(2):181–196. <https://doi.org/10.1016/j.jtbi.2004.06.013>
37. Weng WL, Liu Y, Chen JL, Huang T, Xu LJ, Godoy P, et al. The Etiology of Liver Damage Imparts Cytokines Transforming Growth Factor β 1 or Interleukin-13 as Driving Forces in Fibrogenesis. *Hepathol.* 2009; 50(1):230–243. <https://doi.org/10.1002/hep.22934>
38. Kim Y, Lawler S, Nowicki MO, Chiocca EA, Friedman A. A mathematical model for pattern formation of glioma cells outside the tumor spheroid core. *J Theor Biol.* 2009; 260(3):359–371. <https://doi.org/10.1016/j.jtbi.2009.06.025> PMID: 19596356
39. Terrault NA, Bzowej NH, Chang K, Hwang JP, Jonas MM, Murad MH. AASLD Guidelines for Treatment of Chronic Hepatitis B. *Hepatology: Practice Guideline.* 2015; 00(00):1–23.
40. Maloy KJ, Powrie F. Intestinal homeostasis and its breakdown in inflammatory bowel disease. *Nature.* 2011; 474(7351):298–306. <https://doi.org/10.1038/nature10208> PMID: 21677746
41. Baumgart DC, Carding SR. Inflammatory bowel disease: cause and immunology. *Lancet.* 2007; 369(9573):1627–1640. [https://doi.org/10.1016/S0140-6736\(07\)60750-8](https://doi.org/10.1016/S0140-6736(07)60750-8) PMID: 17499605
42. Albeiroti S, Ayasoufi K, Hill DR, Shen B, de la Motte CA. Platelet hyaluronidase-2: An enzyme that translocates to the surface upon activation to function in extracellular matrix degradation. *Blood.* 2015; 125:1460–1469. <https://doi.org/10.1182/blood-2014-07-590513> PMID: 25411425
43. Baranova A, Lal P, Bireddinc A, Younossi ZM. Non-invasive markers for hepatic fibrosis. *BMC Gastroenterol.* 2011; 11:91. <https://doi.org/10.1186/1471-230X-11-91> PMID: 21849046
44. Greco RM, Iacono JA, Ehrlich HP. Hyaluronic acid stimulates human fibroblast proliferation within a collagen matrix. *J Cell Physiol.* 1998; 177:465–473. [https://doi.org/10.1002/\(SICI\)1097-4652\(199812\)177:3%3C465::AID-JCP9%3E3.0.CO;2-5](https://doi.org/10.1002/(SICI)1097-4652(199812)177:3%3C465::AID-JCP9%3E3.0.CO;2-5) PMID: 9808154
45. Bai Q, An J, Wu X, You H, Ma H, Liu T, et al. HBV promotes the proliferation of hepatic cells via the PDGF-B/PDGFR- β signaling pathway in vitro. *Int J Mol Med.* 2012 Dec; 30(6):1443–50. <https://doi.org/10.3892/ijmm.2012.1148> PMID: 23042547
46. Fan JM, Ng YY, Hill PA, Nikolic-Paterson DJ, Mu W, Atkins RC, et al. Transforming growth factor-beta regulates tubular epithelial-myofibroblast transdifferentiation in vitro. *Kidney Int.* 1999; 56:1455–1467. <https://doi.org/10.1046/j.1523-1755.1999.00656.x> PMID: 10504497
47. Thomas NJ, Watts KL, Akram KM, Forsyth NR, Spiteri MA. Idiopathic pulmonary fibrosis: immunohistochemical analysis provides fresh insights into lung tissue remodelling with implications for novel prognostic markers. *Int J Clin Exp Pathol.* 2012; 5:58–71.
48. Friedman SL. Hepatic stellate cells: Pretean, multifunctional, and enigmatic cells of the liver. *Physiol Rev.* 2008; 88:125–172. <https://doi.org/10.1152/physrev.00013.2007> PMID: 18195085
49. Lu P, Takai K, Weaver VM, Werb Z. Extracellular matrix degradation and remodeling in development and disease. *Cold Spring Harb Perspect Biol.* 2011; 3:1–25. <https://doi.org/10.1101/cshperspect.a005058>
50. Murray LA, Chen Q, Kramer MS, Hesson DP, Argentieri RL, et al. TGF-beta driven lung fibrosis in macrophage dependent and blocked by Serum amyloid P. *Int J Biochem Cell Biol.* 2011; 43:154–162. <https://doi.org/10.1016/j.biocel.2010.10.013> PMID: 21044893
51. Hao W, Komar HM, Hart PA, Conwell DL, Lesinski GB, Friedman A. Mathematical model of chronic pancreatitis. *PNAS.* 2017 March 30; 114(19):5011–5016. <https://doi.org/10.1073/pnas.1620264114> PMID: 28439020
52. Hao W, Rovin BH, Friedman A. Mathematical model of renal interstitial fibrosis. *Proc Natl Acad Sci.* 2014; 111(39):14193–14198. <https://doi.org/10.1073/pnas.1413970111> PMID: 25225370
53. Zan Y, Zhang Y, Tien P. Hepatitis B virus e antigen induces activation of rat hepatic stellate cells. *Biochem Biophys Res Commun.* 2013 June; 435(3):391–6. <https://doi.org/10.1016/j.bbrc.2013.04.098> PMID: 23665329

54. Wada T, Yokoyama H, Matsushima K, Kobayashi K. Monocyte chemoattractant protein-1: does it play a role in diabetic nephropathy? *Nephrol Dial Transplant*. 2003; 18:457–459. <https://doi.org/10.1093/ndt/18.3.457> PMID: 12584260
55. Hong M, Chou Y, Wu Y, Tsai K, Hu C, Jeng K, et al. Transforming growth factor- β 1 suppresses hepatitis B virus replication by the reduction of hepatocyte nuclear factor-4 α expression. *PLoS ONE*. 2012 January; 71(1):1–13.
56. Ciupe SM, Ribiero RM, Nelson PW, Perelson AS. Modeling the mechanisms of acute hepatitis B virus infection. *J Theor Biol*. 2007; 247:23–35. <https://doi.org/10.1016/j.jtbi.2007.02.017> PMID: 17428501
57. Colombatto P, Civitano L, Bizzarri R, Oliveri F, Choudhury S, Gieschke R, et al. A multiphase model of the dynamics of HBV infection in HBeAg-negative patients during pegylated interferon- α 2a, lamivudine and combination therapy. *Anti-viral Therapy*. 2006; 11:197–212.
58. Lewina S, Ribeiro R, Walters T, Lau G, Bowden S, Locarnini S, et al. Analysis of hepatitis B viral load decline under potent therapy: complex decay profiles observed. *Hepatology*. 2001; 34:1012–1020. <https://doi.org/10.1053/jhep.2001.28509>
59. Lau G, Tsiang M, Hou J, Yuen S, Carman W, Zhang L, et al. Combination therapy with lamivudine and famciclovir for chronic hepatitis B infected Chinese patients: a viral dynamics study. *Hepatology*. 2000; 32:394–399. <https://doi.org/10.1053/jhep.2000.9143> PMID: 10915748
60. Ciupe SM, Catlla AJ, Forde J, Schaeffer DG. Dynamics of hepatitis B virus infection: What causes viral clearance? *Mathematical Population Studies*. 2011; 18:87–105. <https://doi.org/10.1080/08898480.2011.564563>
61. Ciupe SM, Ribiero RM, Perelson AS. Antibody Responses during Hepatitis B Viral Infection. *PLoS Comp Biol*. 2014; 10(7):1–16. <https://doi.org/10.1371/journal.pcbi.1003730>
62. Kamyad AV, Akbari R, heydari AA, Heydari A. Mathematical Modeling of Transmission Dynamics and Optimal Control of Vaccination and Treatment for Hepatitis B Virus. *Comp Math Methods Med*. 2014 475451; 2014:1–15. <https://doi.org/10.1155/2014/475451>
63. Zhao S, Su Z, Lu Y. A mathematical model of hepatitis B virus transmission and its application for vaccination strategy in china. *Int J Epidemiol*. 2000 August; 29(4):744–752. <https://doi.org/10.1093/ije/29.4.744> PMID: 10922354
64. Friedman A, Hao W. Mathematical Modeling of Liver Fibrosis. *Mat Biosc Eng*. 2017 February; 14(1):143–164. <https://doi.org/10.3934/mbe.2017010>
65. Siewe N, Yakubu AA, Satoskar AR, Friedman A. Immune Response to Infection by Leishmania: A Mathematical Model. *Mathematical Biosciences*. 2016 March; 276:28–43. <https://doi.org/10.1016/j.mbs.2016.02.015> PMID: 26987853
66. Siewe N, Yakubu AA, Satoskar AR, Friedman A. Granuloma Formation in Leishmaniasis: A Mathematical Model. *J Theor Biol*. 2017 January; 412:48–60. <https://doi.org/10.1016/j.jtbi.2016.10.004> PMID: 27769685
67. Biermer M, Puro R, Schneider RJ. Tumor Necrosis Factor Alpha Inhibition of Hepatitis B Virus Replication Involves Disruption of Capsid Integrity through Activation of NF- κ B. *J Virol*. 2003 April; 77(7):4033–4042. <https://doi.org/10.1128/JVI.77.7.4033-4042.2003> PMID: 12634363
68. Veremeyko T, Siddigui S, Sotnikov I, Yung A, Ponomarev ED. IL-4/IL-13-dependent and independent expression of miR-124 and its contribution to M2 phenotype of monocytic cells in normal conditions and during allergic inflammation. *PLoS One*. 2013 December; 8(12):1–13. <https://doi.org/10.1371/journal.pone.0081774>
69. Geissmann CADFMGGEOJSKSSACGLF. Monitoring of blood vessels and tissues by a population of monocytes with patrolling behavior. *Science*. 2007 Aout; 3(317):666–670.
70. Italiani P, Boraschi D. From Monocytes to M1/M2 Macrophages: Phenotypical vs. Functional Differentiation. *Front Immunol*. 2014 October; 5(514):1–22.
71. Yang J, Zhang L, Yu C, Yang X, Wang H. Monocyte and macrophage differentiation: circulation inflammatory monocyte as biomarker for inflammatory diseases. *Biomark Res*. 2014 January; 2(1):1–9. <https://doi.org/10.1186/2050-7771-2-1> PMID: 24398220
72. Chen HY, Chen ZX, Huang RF, Lin N, Wang XZ. Hepatitis B virus X protein activates human hepatic stellate cells through upregulating TGF β 1. *Genet Mol Res*. 2014 Oct; 13(4):8645–56. <https://doi.org/10.4238/2014.October.27.4> PMID: 25366754
73. Deepak P, Kumar S, Kishore D, Acharya A. IL-13 from Th2-type cells supresses induction of antigen-specific Th1 immunity in a T-cell lymphoma. *Int Immunol*. 2010; 22(1):53–63. <https://doi.org/10.1093/intimm/dxp114> PMID: 19951958
74. Camelo A, Dunmore R, Sleeman MA, Clarke DL. The epithelium in idiopathic pulmonary fibrosis: breaking the barrier. *Front Pharmacol*. 2014; 4(173). <https://doi.org/10.3389/fphar.2013.00173> PMID: 24454287

75. Clarke DL, Carruthers AM, Mustelin T, Murray LA. Matrix regulation of idiopathic pulmonary fibrosis: the role of enzymes. *Fibrogenesis Tissue Repair*. 2013; 6(20). <https://doi.org/10.1186/1755-1536-6-20> PMID: 24279676
76. Janssen HLA, Berk L, Schalm SW, Heijtkink RA, Hess G, Rossol S, et al. Antiviral effect of prolonged intermittent lymphoblastoid alpha interferon treatment in chronic hepatitis B. *Gut*. 1992; 33:1094–1098. <https://doi.org/10.1136/gut.33.8.1094> PMID: 1398234
77. d'Onofrio A, Gandolfi A. The response to antiangiogenic anticancer drugs that inhibit endothelial cell proliferation. *Appl Math Comput*. 2006 October; 181(2):1155–1162.
78. d'Onofrio A, Gandolfi A, Rocca A. The dynamics of tumour-vasculature interaction suggests low-dose, time-dense anti-angiogenic schedulings. *Cell Prolif*. 2009 June; 42(3):317–329. <https://doi.org/10.1111/j.1365-2184.2009.00595.x> PMID: 19438898
79. d'Onofrio A, Gandolfi A. Chemotherapy of vascularised tumours: role of vessel density and the effect of vascular “pruning”. *J Theor Biol*. 2010 May; 264(2):253–265. <https://doi.org/10.1016/j.jtbi.2010.01.023> PMID: 20100496
80. WebMD. Drugs and Medications: HEPSERA. <https://www.webmd.com/drugs/2/drug-64166/hepsera-oral/details> 2005–2018;.
81. Drug com: Know more Be Sure. Adefovir. <https://www.drugs.com/ppa/adefovir.html> 2000–2018;.
82. WebMD. Interferons for Chronic Hepatitis B. <https://www.webmd.com/hepatitis/interferons-for-chronic-hepatitis-b> 2014;.
83. Paul N, Han S. Combination Therapy for Chronic Hepatitis B: Current Indications. *Curr Hepatitis Rep*. 2011; 10:98–105. <https://doi.org/10.1007/s11901-011-0095-1>
84. Crump KS, Hoel DG, Langley CH, Peto R. Fundamental carcinogenic processes and their implications for low dose risk assessment. *Cancer Res*. 1976; 36(9 pt1):2973–1979. PMID: 975067
85. Altshuler B. Modeling of dose-response relationships. *Env Health Perspec*. 1981; 42:23–27. <https://doi.org/10.1289/ehp.814223>
86. Vanderberg LN, Colborn T, Hayes TB, Heindel JJ, Jacobs DR Jr, Lee DH, et al. Hormones and endocrine-disrupting chemicals: low-dose effects nonmonotonic dose responses. *Endocrine Rev*. 2012; 33(3):378–455. <https://doi.org/10.1210/er.2011-1050>
87. Lai X, Friedman A. Combination therapy of cancer with cancer vaccine and immune checkpoint inhibitors: A mathematical model. *PLoS ONE*. 2017 May; 12(5):1–24. <https://doi.org/10.1371/journal.pone.0178479>
88. Dusheiko G. Side effects of alpha interferon in chronic hepatitis C. *Hepatology*. 1997 September; 26(3 Suppl 1):112S–121S. <https://doi.org/10.1002/hep.510260720> PMID: 9305675
89. Huang R, Hao Y, Zhang J, Wu C. Interferon-alpha plus adefovir combination therapy versus interferon-alpha monotherapy for chronic hepatitis B treatment: A meta-analysis. *Hepatol Res*. 2013; 43:1040–1051. PMID: 23356962